약학박사학위논문

미토콘드리아 및 DNA 타겟 광역동 치료를 위한 술폰산벤조티오핀 포피린 합성

Synthesis of 5, 10, 15, 20-Tetrakis(7-sulfanatobenzo[b]thiophene) Porphyrin for Mitochondria and DNA Targeted Photodynamic Therapy

2016년 2월

서울대학교 대학원

약학과 약품분석학전공

Rangasamy Sabarinathan

약학박사학위논문

미토콘드리아 및 DNA 타겟 광역동 치료를 위한 술폰산벤조티오핀 포피린 합성

Synthesis of 5, 10, 15, 20-Tetrakis(7-sulfanatobenzo[b]thiophene) Porphyrin for Mitochondria and DNA Targeted Photodynamic Therapy

지도교수 송 준 명

이 논문을 약학박사학위논문으로 제출함
2016년 2월

서울대학교 대학원
약학과 약품분석학전공
Rangasamy Sabarinathan

Rangasamy Sabarinathan의 약학박사학위논문을 인준함
2016년 2월

위 원 장	박 정 일 (인)
부 위 원 장	정 낙 신 (인)
위 원	노 민 수 (인)
위 원	나 건 (인)
위 원	송 준 명 (인)

Abstract

Porphyrins are rich in applications and it can be called as the colors of life. From the photosynthetic process in plants, to the red hemoglobin that carries oxygen to the cells in our bodies utilize porphyrin molecules. Thus, without any surprise porphyrins are actively explored as tools for wider applications to improve medicine and other biomedical fields. With the aim of improving photodynamic therapy (PDT) in mind, this thesis work examines new synthetic porphyrins for selective targeting of sub-cellular compartments in cancerous cells and execute apoptotic cell death upon PDT, and causing minimal destruction and irritation to normal tissue.

PDT is a phototherapeutic cancer therapy in which a photosensitizer (PS)—light activated drug—absorbs light of specific wavelength and excites to the singlet state. From the excited singlet state, PSs can undergo an internal transition to the excited triplet state, a relatively long-lived and high-energy species that transfers its excess energy to molecular oxygen. Subsequently, molecular oxygen excites from the stable triplet state to the highly reactive singlet state. With no spin-state restriction, singlet oxygen is cytotoxic, readily reacting with electron-rich biomolecules such as unsaturated lipids, amino acids and DNA consequently destroying the tumor cell. Singlet

oxygen has a limited range of diffusion. Therefore, the site of its generation is also the site of initial damage.

Photosensitizers used in PDT are often classified as first, second and third generation PS. This classification is based on the historical development and conceptual approaches. Haematoporphyrin derivative (HpD) or Photofrin are otherwise called as first generation PS enjoyed its success in cancer therapy due to their tumor localizing and photophysical properties yet suffers from its drawbacks (mixture of compounds and less selectivity). Herein, second generation PSs with high purity and improved photophysical properties had been developed. Still there is always room for improver, and current research efforts are aimed at developing third generation PSs where additional biological criteria such as selective targeting of sub-cellular organelles are considered in the design principle.

Herein, this thesis work focused in developing third generation PSs that can target selectively sub-cellular organelles such mitochondria and DNA and effectively induce apoptotic cell death after PDT. In Chapter I, a comprehensive background on history of photodynamic therapy, fundamental aspects, classification and requirements of PSs is presented. In chapter 2, synthesis, structural elucidation, photophysical properties and *in*

vitro photokilling and mechanism of cell death of 5, 10, 15, 20–Tetrakis(7-sulfonatobenzo[b]thiophene)porphyrin (SBTP) is studied.

Keywords: porphyrin; photosensitizers; photodynamic therapy; mitochondria; DNA; apoptosis; intrinsic; extrinsic; high-content assay.

Student number: 2010-31366

Table of Contents

List of Figures

List of Tables

List of Abbreviations

PDT: Photodynamic therapy

PSs: Photosensitizers

HpD: Haematoporphyrin derivative

SBTP: 5, 10, 15, 20–Tetrakis(7-sulfonatobenzo[b]thiophene)porphyrin

BTP: 5, 10, 15, 20–Tetrakis(Benzo[b]thiophene)porphyrin

LDC: Least developed countries

$^1O_2$: Singlet oxygen

ROS: Reactive oxygen species

S_0: Singlet ground state

S_1: First excited singlet-state

T_1: First excited triplet state

MPT: Mitochondrial permeability transition

HCA: High-content cell-based assay

CSA: Chlorosulfonic acid

TPP: Tetraphenyl porphyrin

DPBF: 1, 3-diphenylisobenzofuran

MTT: 3-(4,5-dimethylthiazol-2-yl)-2,5-diphenyltetrazolium bromide

DCFDA: 2'-7'- dicholofluorescein-diacetate

BTS: Benzo[b]thiophenesulphonamide 1,1-dioxide

Chapter I

Introduction

1.0. Cancer

Cancer is a dreadful disease that varies in rate of growth, state of cellular differentiation, diagnostic detectability, invasiveness, metastatic potential and response to treatment and prognosis. Cancer occur when cells become abnormal and keep dividing, forming new cells without any control or order. All organs of the body are made up of cells. Normally, cells divide to form new cells only when the body needs them. When cells divide uncontrollably a mass of excess tissue is formed called a tumor. Tumors can be non-cancerous (benign) or cancerous (malignant). If cells are malignant they can invade and damage neighboring tissue and organs. These malignant cells can also travel into the blood stream to form new tumors in other parts of the body this process is known as metastasis.

Cancer can occur at any time and is impartial of age and sex. In 2012, there were 8.2 million causalities, and the least developed countries (LDCs) contributed 57% and 65% to the worldwide cancer incidence and mortality,

respectively.[1] However, through better diagnostic techniques and improved treatment millions of people have been treated and cured.

1.0.1. Causes of cancer

In many cases, the causes of cancer are not clear; however, both external and internal factors play a role. Cigarette smoking is a major casual factor of lung cancer. Diets, genetic mutation, infection, sexual behavior, exposure to ultraviolet light and carcinogenic chemicals have also been implicated in other forms of cancer.

1.0.2. Cancer prevention

The best way to reduce deaths from cancer is to prevent it. Doctors generally agree that about one third of all human cancers are directly related to cigarette smoking. For a smoker, the risk of cancer is much higher than that of a nonsmoker. The next most commonly cited cancer causing factor is diet. The National Cancer Institute and the American Cancer Society recommended a diet low in fat, high in fiber, and rich in fruits and vegetables can prevent cancer. Chemoprevention on the other hand is simply prevention with drugs. The word “drugs” is used to include dietary

supplements, hormones, and vitamins etc., as well as real drugs, synthetic and natural agents used for therapeutic purposes. The number of chemoprevention agents is increasing.[2]

1.0.3. Cancer Treatments

There are many types of cancer treatment. The types of treatment varies depending on the type of cancer and how advanced it is. Surgery is still the oldest and most common treatment method for the removal of malignant tumors. Radiation therapy is another method used to treat cancer. But most people have a combination of treatments, such as surgery with chemotherapy and/or radiation therapy. Other treatments include hormone therapy, targeted therapy, radiation therapy and photodynamic therapy.

1.2. Photodynamic Therapy

1.2.1. History of Photodynamic therapy

For more than three thousand years light has been used as a therapy.[3, 4] Indian, Egyptian and Chinese civilizations had used light to treat diseases such as psoriasis, rickets and skin cancers.[5] Although the therapeutic

properties of light were known in ancient civilizations, the importance of the light treatment for cutaneous diseases started to be recognized at the beginning of the last century when Niels Finsen received the Nobel Prize in this field. The concept of photodynamic action also dates back to more than 100 years ago when Oscar Raab reported that certain wavelengths were lethal to infusoria — including a species of Paramecium— in the presence of acridine.[6] Later in the year 1903, Herman Von Tappeiner and A. Jesionek treated skin tumours with topically applied eosin and white light.[7] Also, they described this phenomenon as 'PHOTODYNAMIC ACTION' (see timeline in Figure 1).

The modern explosion of interest in PDT began with the discovery and study of hematoporphyrin derivative (HpD) by Lipson and Schwartz at the Mayo Clinic in 1960,[8, 9] and accelerated by pioneering studies in both basic science and clinical application by Dougherty et al.[10] In 1983, a partially purified form of hematoporphyrin derivative (HpD), now commercially known as Photofrin (porfimer sodium; QLT, Vancouver, BC, Canada), was developed. Photofrin was the first PS to receive regulatory approval for treatment of various cancers in more than 40 countries throughout the world, including the United States (by Food and Drug Administration in 1995).

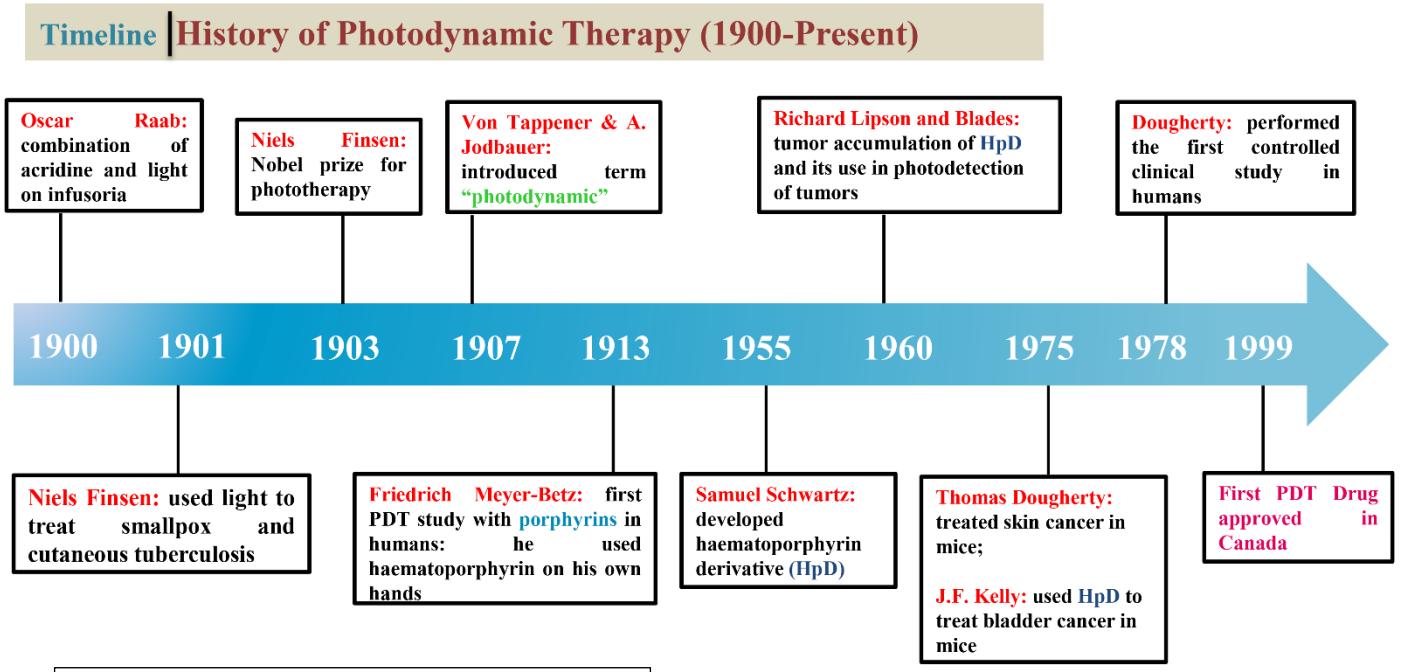

Figure 1. History of photodynamic therapy

Photodynamic therapy (PDT) consists of the administration and selective accumulation of a photosensitizer (PS) in target tumor tissues, followed by generation of singlet oxygen ($^1O_2$) and other cytotoxic reactive oxygen species (ROSs) that result in cell membrane damage and subsequent cell death upon irradiation with light of appropriate wavelength in the presence of tissue oxygen (**Figure 2**).

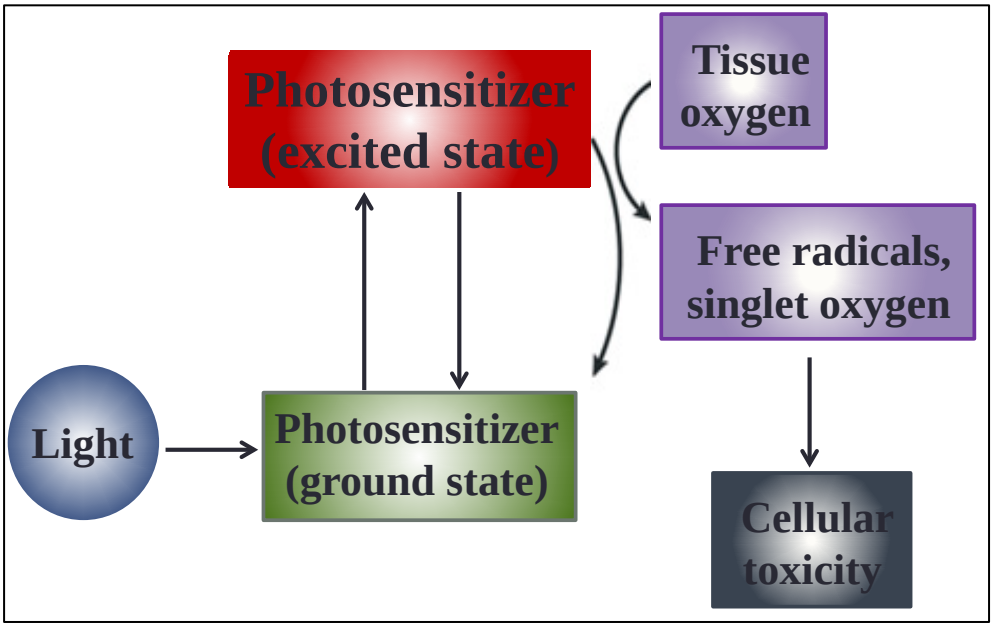

Figure 2. Mechanism of action of photodynamic therapy

1.2.1. Basic principles of PDT

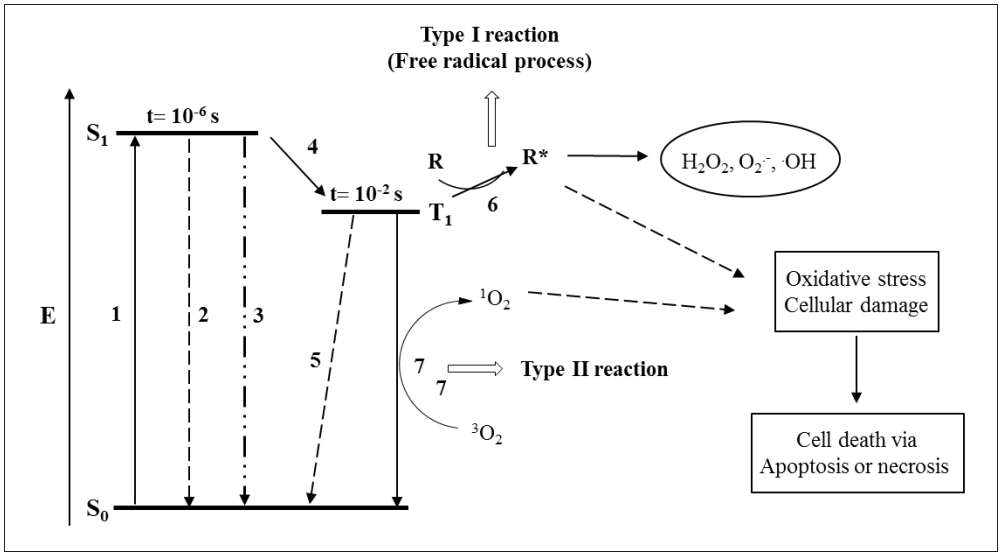

Figure 3. Modified Jablonski diagram. Photophysical processes involved in photodynamic therapy: 1) absorption, 2) fluorescence, 3) internal conversion, 4) intersystem crossing, 5) phosphorescence, 6) formation of free radicals by energy transfer from T1 photosensitizer.

The basic photophysical processes involved in PDT are illustrated in **Figure 3**.[11] The PS is activated from its singlet ground state (S_0) to the short-lived first excited singlet-state (S_1) upon absorption of light with appropriate wavelengths. 2) The S_1 PS can return to the S_0-state by emitting the absorbed energy as fluorescence or 3) by internal conversion. 4)

Alternatively, it can also convert to the relatively long-lived first excited triplet state (T_1) by intersystem crossing. 5) The T_1 PS can return to the S_0-state by emitting phosphorescence. However, energy transfer from T_1 to biological substrates or molecular oxygen generates ROSs ($^1O_2$, H_2O_2, $O_2^{\bullet-}$, $^{\bullet}OH$), which produce cellular damage to death mainly by necrosis or apoptosis method.

There are two proposed types of photochemical pathways, known as type I and type II reactions (**Scheme 1**).[12]

Type I mechanism	**Type II mechanism**
$^3Ps^* + O_2 \rightarrow Ps^{\bullet+} + O_2^{\bullet}$	$Ps \rightarrow {}^1Ps^* \rightarrow {}^3Ps^*$
$^3Ps^{\bullet} + \text{substrate} \rightarrow Ps^{\bullet} + \text{substrate}^{\bullet+}$	$^3Ps^* + {}^3O_2 \rightarrow Ps + {}^1O_2$
$Ps^{\bullet} + O_2 \rightarrow Ps + O_2^{\bullet}$	$^1O_2 + \text{substrate} \rightarrow \text{oxidation}$
$O_2^{\bullet} \rightarrow HO_2^{\bullet}$	
$HO_2^{\bullet} + \text{substrate-H} \rightarrow H_2O_2 + \text{substrate}\bullet$	

Scheme 1. Type I and Type II mechanisms.

In the type I reaction, the PS interacts with a biomolecule (or oxygen) resulting in hydrogen atom (or electron) transfer that leads to the production of free radicals. In the type II reaction, singlet oxygen is generated as a result of energy transfer from the T_1 PS to the triplet ground state of

molecular oxygen. Although these two pathways could be occurred in the photosensitization process, however, it is suggested that the type II predominates over the others, in that singlet oxygen shows relatively high reactive property and causes irreversible destruction of tumor cells.

1.2.2. Mechanisms of tumour destruction

It has been postulated that three mechanisms could be involved in the irreversible damage of tumour tissue when treated with PDT. These include the following:

1) Direct killing of malignant cells, largely as a consequence of impairment of mitochondrial functions and the alteration of mitochondrial/cytoplasmic membranes.
2) Indirect cell killing due to photodynamic damage or shutdown of the (neo) vascular with loss of oxygen and nutrients to the tumour owing to disruption of the endothelium.
3) Additional anti-tumour contributions from the inflammatory and immune response of the host.

Although all three are thought necessary for the best long term response, their relative roles will vary considerably depending on the photosensitiser,

its sub cellular and tissue distribution, the tumour type and its microvasculature, and the type and duration of the inflammatory and immune response elicited in the host.[13] Also, as a consequence of PDT the singlet oxygen generated by the photosensitiser will affect practically all of the cellular organelles due to the wide and varied sensitiser distribution within the cells. Subsequently, because there are multiple cellular targets for the singlet oxygen it has been proved difficult to distinguish between the events leading up to cell death. However, with the ongoing development in this area, more sensitive techniques are becoming available for the detection of photosensitiser in cells. With the use of innovative molecular and biochemical strategies the mapping of cellular events before and after photosensitisation, is bringing some clarity to the process of cell death via toxic oxygen treatment. Although there are multiple cellular targets available to the toxic oxygen one of the cellular components that has been studied and targeted by PDT in preference to others is the mitochondria.[14]

1.3. Sensitizers

Numerous sensitizers produce singlet oxygen and can be considered suitable for PDT, nevertheless, the majority of sensitizers investigated in this context

were compounds with a porphyrinoid structure.[15-18] The reason for this preference is the extensive knowledge of their chemistry together with the inherent similarity to natural porphyrins frequently occurring in living matter. Of non-porphyrinoid sensitizers eosine, acridine, rose bengal, methylene blue, perylenequinones, triarylmethane dyes, etc. have been taken into consideration. The effort to correlate the structure of the sensitizer to intermolecular non-covalent interactions produced a categorical requirement to use well-defined individual sensitizers. Mixtures of derivatives, species differing in the number of substituents or even different regioisomers, interacting differently with biomolecules in the tissue, often yield misleading results on structure–activity relationships. Sensitizers suitable for PDT have to meet a number of specific requirements:

- ***Maximum absorption in the region 600–800 nm[15, 18]***

  The incident intensity of light—irradiance—is reduced by absorption by chromophores in tissue or by scattering. The efficiency of scattering increases as the wavelength is decreased. On the other side, absorption by water molecules increases at wavelengths above 800 nm. Consequently, the window for optimum penetration lies between 600 and 800 nm, i.e. in the region of red light. The characteristic

quantity is the penetration depth δ defined as the depth in which the irradiance is reduced to 1/e of the initial value. Typical values of δ vary between 1 and 3 mm, but apparently the photodynamic effect reaches beyond this limit. The upper limit of the wavelength to produce $^1O_2$ is given by the energy necessary for the $^1O_2$ formation ($\lambda < 1269$ nm, $\Delta E > 94.1$ kJ mol^{-1} for a one-photon process).

- ***Minimum absorption in the region 400–600 nm[19]***

  Sensitizers absorbing in this region, i.e. in the maximum of the spectroscopic distribution of daylight, enhance photosensitivity of the skin, which is a complicating side effect of photodynamic treatment. Photosensitization of skin has been the major drawback of first generation sensitizers based on hematoporphyrin derivatives.

- ***High quantum yields of $^1O_2$***

  The quantum yields Φ_Δ vary in the range 0.3–0.8 for most sensitizers. The significance of Φ_Δ should not be overestimated, since the amount of $^1O_2$ produced depends strongly on other factors, namely on interaction of the sensitizer with surrounding biopolymers, aggregation of the sensitizer, oxygen depletion and side reactions. The demand of high Φ_Δ includes the prerequisite of adequately high

Φ_T, the triplet state energy sufficient for the $^1O_2$ formation and relatively long lifetime of the triplet states τ_T.

- ***Photostability***

  A sensitizer should be stable against photodegradation and against oxidation by $^1O_2$ or other reactive oxygen species generated in situ. Photobleaching of sensitizers in biological systems is a complex process, not necessarily oxygen dependent. Photobleaching plays an important role in decreasing skin sensitization and the specificity of phototreatment.[15, 16]

- ***Non-toxicity and phototoxicity***

  Low "dark" toxicity (e.g. nephrotoxicity, neurotoxicity) is desirable so as to avoid unnecessary strain on the organism prior to irradiation. The overall destructive photodynamic effect of the sensitizer on biological material in vitro or in vivo is called phototoxicity.

- ***Specific retention in the malignant tissue***

  The specific retention of a sensitizer in the malignant tissue is a consequence of different kinetics of sensitizer removal from the malignant and healthy tissue. The removal from the healthy tissue is faster. The concentration difference is adjusted within several hours

after sensitizer administration and depends on the nature of the sensitizer. Effectual removal of the sensitizer from the healthy tissue precludes its photodynamic damage.[20]

- ***Single substance***

  The use of a single, well-defined substance is necessary for reliable evaluation of the sensitizer–biopolymer interaction.

- ***Fluorescence***

  Fluorescence of the sensitizer enables detection of the sensitizer distribution in vivo. To retain both functions of the sensitizer, namely fluorescence and $^1O_2$ production, the ratio Φ_f/Φ_{isc} should be optimized.

- ***Solubility***

  Sufficient solubility of the sensitizer in aqueous media is important for direct intravenous application and transport to the intended target location. Hydrophobic, insoluble sensitizers can be transported by water-soluble carriers.

1.3.1. Porphyrinoid photosensitizers

Basic skeletons of porphyrinoid PSs are presented in **Figure 4**. Structures 1–4 were originally natural products, whose synthetic analogues are used as a

rule. Synthetic porphyrins **1** are often substituted in the meso-positions. Chlorin **2** and bacteriochlorin **3** are partly hydrogenated porphyrins; hydrogenation shifts the absorption bands to the more advantageous region above 600 nm. Purpurins **4** are degradation products of chlorophylls. Compounds **5–11** are purely synthetic and have no counterpart in nature. Porphyrazine or tetraazaporphyrin **5** is the basic skeleton of the extensively used phthalocyanines **6** and naphthalocyanines **7**.[21] Among novel types of porphyrinoid compounds **8–11** are new sensitizers, some of which are very promising for PDT. Porphycenes **8** are isomeric porphyrins with differing length of the pyrrole–pyrrole bridges.[22, 23] Expanded porphyrins **9** are characterized by an increased number of atoms separating the pyrrole rings. The most important expanded porphyrins are sapphyrins **10** and texaphyrins **11**.[17, 18, 24]

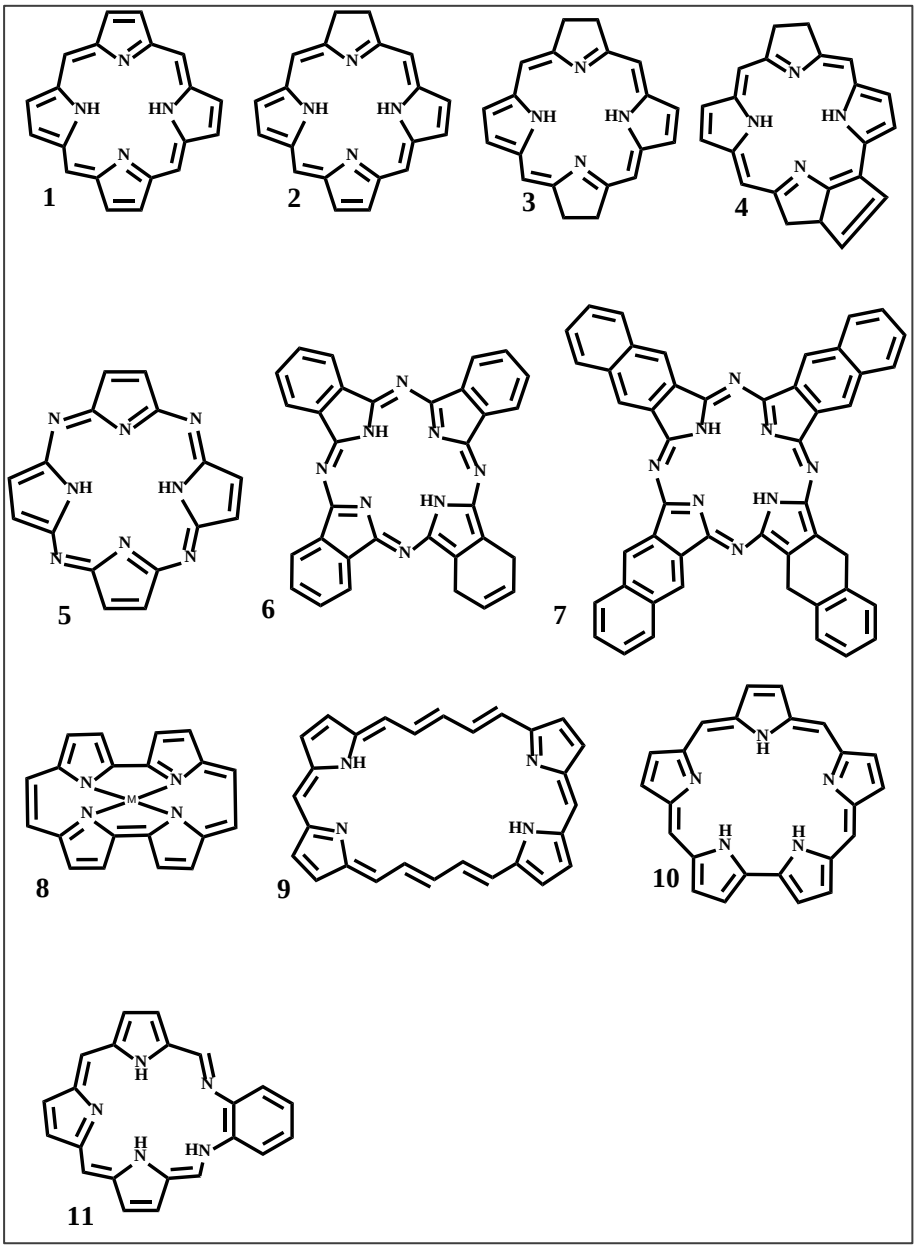

FIGURE 4. Basic structures of porphyrinoid sensitizers**.**

Generally, porphyrinoid sensitizers can be free ligands or metallocomplexes with Al, Zn, Mg, Ga, Si, Ge, Sn, or lanthanides central ions. Meso-substituted porphyrins, chlorins and some expanded porphyrins are usually applied as free ligands (non-metallated). On the other hand, phthalocyanines and naphthalocyanines are always metallated since the free ligand is less chemically stable. Complexes with transition metals are poor sensitizers because of their short triplet lifetimes ranging from picoseconds to nanoseconds.

1.4. Classification of photosensitizers

Photosensitizers are generally classified as the first, second and third generations.[25] The first generation PSs include HpD and Photofrin. The second generation PSs has been developed since the late 1980s to overcome the disadvantages of the first generation PSs. The third generation PSs are referred to those second generation PS conjugates coupled on carriers such as cholesterol, antibodies, and liposomes for selective accumulation and targeting within tumor tissue.[26]

1.4.1. First Generation Photosensitizers

Hematoporphyrin and its chemical derivatives; hematoporphyrin derivative (HpD), and its purified forms Photofrin®, Photosan® and Photochem®, were the first photosensitisers employed in PDT and are referred to as first generation photosensitisers (**Figure 5**).113

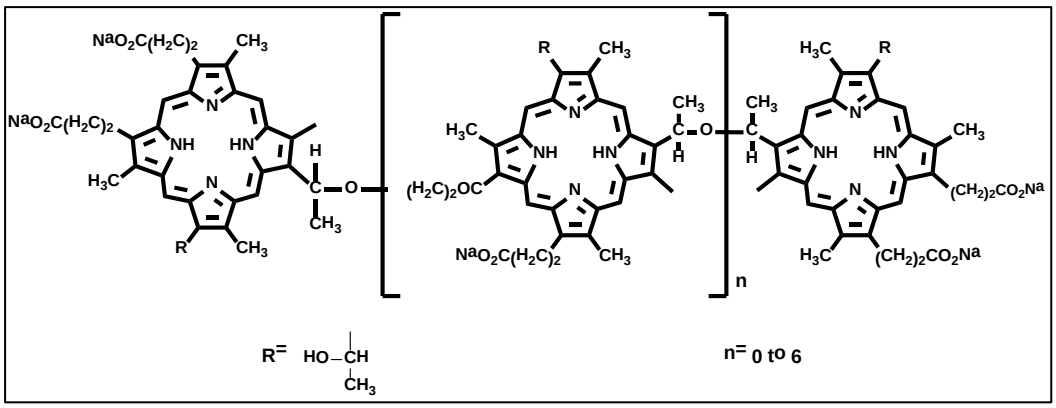

Figure 5. Photofrin® is presented as a mixture of purified fractions of hematoporphyrin derivatives

However, although these photosensitisers are known to selectively accumulate in a variety of solid tumours for prolonged periods of time, they do suffer from three major drawbacks.

- Low selectivity between tumours and peritumoral tissue, consequently, skin photosensitivity is a major side effect.

- Absorption in the red region is weak i.e. 630nm, and so deep tumours are difficult to treat.
- PSs are a mixture of at least 12 components.

1.4.2. The Second Generation of Photosensitizers

The first generation PS Photofrin has been shown to be efficacious in the treatment of many cancer types; however it has some drawbacks as discussed in the above section. Therefore, to overcome these drawbacks and improve the treatment efficacy, several strategies have been employed for the development of more tumor-selective agents with reduced side effects, especially skin phototoxicity. Some of the second generation PSs have recently been developed and were introduced in clinical trials. Most of them are cyclic tetrapyrroles, comprising substituted derivatives of porphyrin, chlorin, and bacteriochlorin. Examples of these PSs are shown in **Figure 6**, including Tookad (palladium bacteriopheophorbide; MedKoo Biosciences, Chapel Hill, NC, USA; Fig 1A), Antrin (Lu texaphyrin, a tripyrrole expanded macrocycle; Pharmacyclics Inc., Sunnyvale, CA, USA; Fig. 1B), benzoporphyrin derivative monocarboxylic acid (BPD-MA; Fig. 1C),

Purlytin (Tin ethyl etiopurpurin; Miravant Medical Technologies, Santa barbara, CA, USA; Fig. 1D), Foscan (meso-tetrahydroxyphenyl chlorine; Biolitec Pharma Ltd., Dublin, Ireland; Fig. 1E), and zinc (II) phthalocyanine (Pc; Fig. 1F), all of which have strong absorption at 650 to -750 nm.[27]

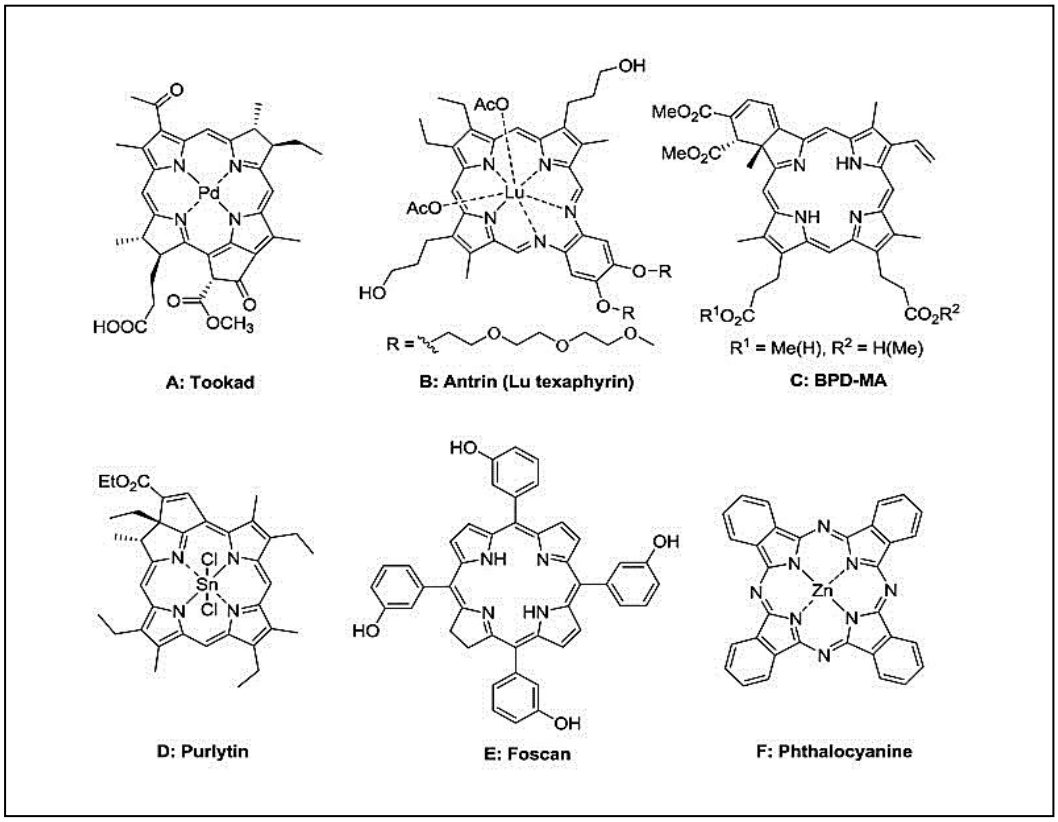

Figure 6. Examples of second generation photosensitizer. (A) Tookad. (B) Antrin (Lu texaphyrin). (C) Benzoporphyrin derivative monocarboxylic acid (BPD MA). (D) Purlytin. (E) Foscan. (F) Phthalocyanine

Due to strong absorption (675 to 800 nm) by the second generation of PS, were able to penetrate deep into the tissues to a depth of up to 2-3 cm. The interpretation of dose-response relationships for these PS is easier because they are not mixtures of compounds. In order to have good photophysical properties, these PS should either be metal-free or contain metal ions with closed d-electron shell configurations (Zn^{II}, AI^{III}, Si^{IV}, Ge^{lV}). A potential photosensitizer should be discussed in terms of its photophysical and photochemical properties, structure (hydrophobicity/hydrophilicity), and stability. Most PS of the second generation absorb at $\lambda > 675$ nm with $\varepsilon >$ 50000 L mol^{-l} cm^{-1}. Singlet oxygen quantum yields are higher than 0.3. Since the diffusion distance of singlet oxygen in cells during its lifetime is less than 100 nm, local damage can be expected at its sites of origin.[28] Therefore, in principle, the photodynamic activity of the aforementioned PS directly depends not on their $^1O_2$ quantum yields but on their different uptake mechanism and subsequent intracellular concentration and localization.[29]

1.4.3. The Third Generation Photosensitizers

In addition to the characteristics of the second generation PS, photosensitizers of the third generation should have properties providing selective delivery of PS to the tumor tissue. Conjugating a targeting component, such as an antibody (directed against the tumour antigens), towards the photosensitizer allows the drug to localize, accumulate and bind selectively at the diseased site **(Figure 7).**[30-32]

The photosensitizer bioconjugate is then able to (specifically) photodynamically inactivate in tumour cells expressing the tumour-associated antigen, minimizing healthy cell localization and concomitant damage. Other receptor-positive sites on the tumour surface, such as LDLs (low-density lipoproteins) and folate receptors could be taken advantage of by conjugating the photosensitizer to LDL or folate molecules[30]: LDL and folate receptors are overexpressed on tumour cell surfaces. An alternative approach would be to use a molecular carrier such as a liposome or targeted nanospecies.[30, 33] Attaching targeting components to the photosensitizer also has an additional benefit. A number of photosensitizers that have shown promise in vivo exhibit poor solubility in aqueous media, preventing

intravenous delivery into the bloodstream and affecting their efficacy and use in physiological media and the clinic.

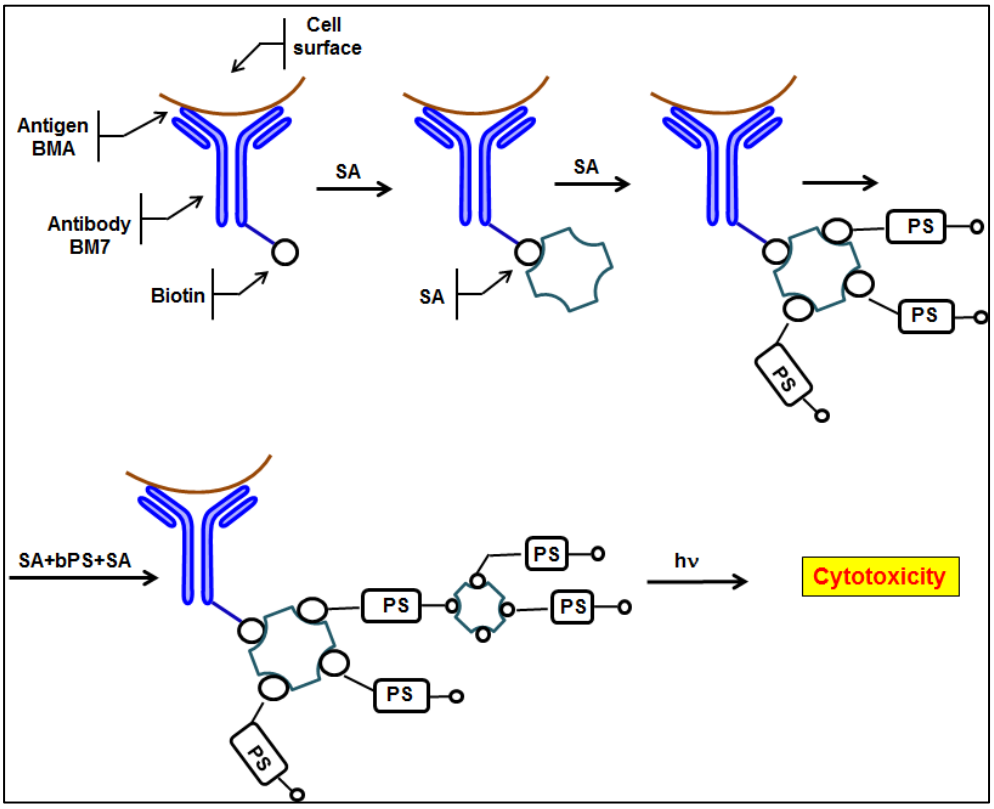

Figure 7. Schematics showing mAB--PS conjugate that bind specifically to the tumor tissue and sensitize its photokilling without damaging normal tissues.

The chemical structure of a photosensitizer plays a key role in the success of the compound as a PDT agent. Photosensitizers need to be soluble in

physiological media: the degree of photosensitizer hydrophilicity and amphiphilicity directly affects its route of administration and the biodistribution/pharmacokinetic profile.[33, 34] Photosensitizers bearing certain structural characteristics have been reported to localize selectively in tumour tissue. Although the localization mechanisms are not fully understood, the more hydrophobic photosensitizers have demonstrated tumour to normal tissue ratios of 7:1 and 8:1, whereas the equivalent hydrophilic photosensitizers exhibited a 2:1.[35] Photosensitizers with anionic substituents, such as sulphonate or carboxyl groups, have been observed to localize preferentially in the cytoplasm and relocate to the nucleus upon illumination,[36] whereas lipophilic photosensitizers functionalized with cationic groups are believed to (preferentially) traverse the mitochondrial membrane and accumulate in the mitochondrion[37]— the subcellular organelle widely demonstrated to be a key component in the preferred (apoptotic) cell death pathway. Exactly which physicochemical/structural properties and mechanisms are behind these specific distributions and localizations and how to maximize tumour tissue selectivity over normal tissue accumulation are issues still under investigation.

References

1. Ferlay, J.; Soerjomataram, I.; Dikshit, R.; Eser, S.; Mathers, C.; Rebelo, M.; Parkin, D. M.; Forman, D.; Bray, F. Cancer incidence and mortality worldwide: sources, methods and major patterns in GLOBOCAN 2012. *Int J Cancer* **2015,** 136, E359-86.

2. Noble, R. L. The discovery of the vinca alkaloids--chemotherapeutic agents against cancer. *Biochem Cell Biol* **1990,** 68, 1344-51.

3. Daniell, M. D.; Hill, J. S. A history of photodynamic therapy. *Aust N Z J Surg* **1991,** 61, 340-8.

4. Ackroyd, R.; Kelty, C.; Brown, N.; Reed, M. The history of photodetection and photodynamic therapy. *Photochem Photobiol* **2001,** 74, 656-69.

5. Spikes, J. The Historical Development of Ideas on Applications of Photosensitized Reactions in the Health Sciences. In *Primary Photo-Processes in Biology and Medicine*, Bensasson, R. V.; Jori, G.; Land, E. J.; Truscott, T. G., Eds. Springer US: 1985; pp 209-227.

6. Dolmans, D. E.; Fukumura, D.; Jain, R. K. Photodynamic therapy for cancer. *Nat Rev Cancer* **2003,** 3, 380-7.

7. von Tappeiner, H.; Jesionek, A. Therapeutische Versuche mit fluoreszierenden Stoffen. *Münchner Med Wochenschr* **1903,** 50, 2042-2044.

8. Lipson, R. L.; Baldes, E. J. The photodynamic properties of a particular hematoporphyrin derivative. *Arch Dermatol* **1960,** 82, 508-16.

9. Lipson, R. L.; Baldes, E. J.; Olsen, A. M. The Use of a Derivative of Hematoporphyrin in Tumor Detection. *Journal of the National Cancer Institute* **1961,** 26, 1-11.

10. Dougherty, T. J.; Grindey, G. B.; Fiel, R.; Weishaupt, K. R.; Boyle, D. G. Photoradiation therapy. II. Cure of animal tumors with hematoporphyrin and light. *J Natl Cancer Inst* **1975,** 55, 115-21.

11. Sternberg, E. D.; Dolphin, D.; Brückner, C. Porphyrin-based photosensitizers for use in photodynamic therapy. *Tetrahedron* **1998,** 54, 4151-4202.

12. Foote, C. S. Definition of type I and type II photosensitized oxidation. *Photochemistry and photobiology* **1991,** 54, 659-659.

13. Jori, G. Tumour photosensitizers: approaches to enhance the selectivity and efficiency of photodynamic therapy. *Journal of Photochemistry and Photobiology B: Biology* **1996,** 36, 87-93.

14. Morgan, J.; Oseroff, A. R. Mitochondria-based photodynamic anti-cancer therapy. *Adv Drug Deliv Rev* **2001,** 49, 71-86.

15. Boyle, R. W.; Dolphin, D. Structure and biodistribution relationships of photodynamic sensitizers. *Photochem Photobiol* **1996,** 64, 469-85.

16. Macdonald, I. J.; Dougherty, T. J. Basic principles of photodynamic therapy. *Journal of Porphyrins and Phthalocyanines* **2001,** 5, 105-129.

17. Ali, H.; Van Lier, J. E. Metal complexes as photo-and radiosensitizers. *Chemical Reviews* **1999,** 99, 2379-2450.

18. Bonnett, R. Photosensitizers of the porphyrin and phthalocyanine series for photodynamic therapy. *Chemical Society Reviews* **1995,** 24, 19-33.

19. Jori, G. Far-red-absorbing photosensitizers: their use in the photodynamic therapy of tumours. *Journal of Photochemistry and Photobiology A: Chemistry* **1992,** 62, 371-378.

20. Henderson, B. W.; Dougherty, T. J. How does photodynamic therapy work? *Photochemistry and photobiology* **1992,** 55, 145-157.

21. Wöhrle, D.; Gitzel, J.; Okura, I.; Aono, S. Photoredox properties of tetra-2, 3-pyridinoporphyrazines (29 H, 31 H-tetrapyrido [2, 3-b: 2′, 3′-g: 2 ″,

3 ″-l: 2 [triple prime], 3 [triple prime]-q] porphyrazine). *Journal of the Chemical Society, Perkin Transactions 2* **1985**, 1171-1178.

22. Vogel, E.; Köcher, M.; Schmickler, H.; Lex, J. Porphycene—a novel porphin isomer. *Angewandte Chemie International Edition in English* **1986,** 25, 257-259.

23. Vogel, E. Novel porphyrinoids. *Pure and applied chemistry* **1990,** 62, 557-564.

24. Jasat, A.; Dolphin, D. Expanded porphyrins and their heterologs. *Chemical reviews* **1997,** 97, 2267-2340.

25. O'Connor, A. E.; Gallagher, W. M.; Byrne, A. T. Porphyrin and nonporphyrin photosensitizers in oncology: preclinical and clinical advances in photodynamic therapy. *Photochemistry and photobiology* **2009,** 85, 1053-1074.

26. Allison, R. R.; Sibata, C. H. Oncologic photodynamic therapy photosensitizers: a clinical review. *Photodiagnosis and photodynamic therapy* **2010,** 7, 61-75.

27. Castano, A. P.; Demidova, T. N.; Hamblin, M. R. Mechanisms in photodynamic therapy: part one—photosensitizers, photochemistry and

cellular localization. *Photodiagnosis and photodynamic therapy* **2004,** 1, 279-293.

28. Moan, J.; BERG, K. The photodegradation of porphyrins in cells can be used to estimate the lifetime of singlet oxygen. *Photochemistry and photobiology* **1991,** 53, 549-553.

29. Kimel, S.; Tromberg, B.; Roberts, W.; Berns, M. Singlet oxygen generation of porphyrins, chlorins, and phthalocyanines. *Photochemistry and photobiology* **1989,** 50, 175-183.

30. Konan, Y. N.; Gurny, R.; Allémann, E. State of the art in the delivery of photosensitizers for photodynamic therapy. *Journal of Photochemistry and Photobiology B: Biology* **2002,** 66, 89-106.

31. Hudson, R.; Carcenac, M.; Smith, K.; Madden, L.; Clarke, O.; Pelegrin, A.; Greenman, J.; Boyle, R. The development and characterisation of porphyrin isothiocyanate–monoclonal antibody conjugates for photoimmunotherapy. *British journal of cancer* **2005,** 92, 1442-1449.

32. Staneloudi, C.; Smith, K. A.; Hudson, R.; Malatesti, N.; Savoie, H.; Boyle, R. W.; Greenman, J. Development and characterization of novel photosensitizer: scFv conjugates for use in photodynamic therapy of cancer. *Immunology* **2007,** 120, 512-517.

33. Castano, A. P.; Demidova, T. N.; Hamblin, M. R. Mechanisms in photodynamic therapy: part three—photosensitizer pharmacokinetics, biodistribution, tumor localization and modes of tumor destruction. *Photodiagnosis and Photodynamic Therapy* **2005,** 2, 91-106.

34. Macdonald, I. J.; Dougherty, T. J. Basic principles of photodynamic therapy. *Journal of Porphyrins and Phthalocyanines* **2001,** 5, 105-129.

35. Rück, A.; Steiner, R. Basic reaction mechanisms of hydrophilic and lipophilic photosensitisers in photodynamic tumour treatment. *Minimally Invasive Therapy & Allied Technologies* **1998,** 7, 503-509.

36. Patito, I. A.; Rothmann, C.; Malik, Z. Nuclear transport of photosensitizers during photosensitization and oxidative stress. *Biology of the Cell* **2001,** 93, 285-291.

37. Dummin, H.; Cernay, T.; Zimmermann, H. Selective photosensitization of mitochondria in HeLa cells by cationic Zn (II) phthalocyanines with lipophilic side-chains. *Journal of Photochemistry and Photobiology B: Biology* **1997,** 37, 219-229.

Chapter II

Synthesis and Photodynamic Studies of Novel *meso*-Substituted Benzo[b]thiophene Porphyrins

Abstract

Photodynamic therapy (PDT) selectively targets subcellular organelles promises an excellent therapeutic strategy for cancer treatment. Here, we synthesized a new water-soluble photosensitizer, 5, 10, 15, 20-Tetrakis (7-sulfonatobenzo[b]thiophene) Porphyrin (SBTP). Rational design of the porphyrinic molecule containing Benzo[b]thiophene moiety at the *meso*-position led to selective accumulation in both mitochondria and nucleus of MCF-7 cells. This multi-target ability of SBTP can cause damage to mitochondria as well as DNA simultaneously. FACS analysis showed rapid cellular uptake of SBTP. High-content cell-based assay was executed to concurrently monitor increase of cytosolic Ca^{2+} levels, mitochondrial permeability transition (MPT), and caspase-3/7/8 activation in MCF-7 cells under the pathological condition caused by PDT action of SBTP. The study of cell death dynamics showed that PDT action of SBTP caused a

significant level of MPT followed by an increase in cytosolic Ca^{2+} level. The localization of SBTP in the mitochondria activated the intrinsic apoptotic pathway. On the other hand, localization of SBTP in the nucleus led to DNA damage in MCF-7 cells. The DNA fragmentation that occurred by PDT action of SBTP was thought to be responsible for extrinsic apoptosis of MCF-7 cells.

Keywords: porphyrin; photodynamic therapy; apoptosis; mitochondria; nucleus; high-content assay.

2.0. Introduction

Cancer is a devastating illness and a major cause of death worldwide. In 2012, there were 8.2 million causalities, and the least developed countries (LDCs) contributed 57% and 65% to the worldwide cancer incidence and mortality, respectively.[1] The common treatment strategies for cancer include surgery, chemotherapy, radiation, and targeted therapy. Among them, photodynamic therapy (PDT) has been reported as a potential and noninvasive treatment strategy for different types of cancer.[2-5] In many countries regulatory approvals have been granted for the clinical use of photosensitizers and PDT light therapies in cancer treatments. Photofrin obtained its first regulatory approval for recurrent papillary tumors in Canada in 1993 and in Japan in 1994, it has been used to treat carcinoma *in situ* and dysplasia of the uterine cervix.[6] PDT is a light-activated therapy that combines three non-toxic components: a light source, a photosensitizer (PS), and molecular oxygen of the cell. The mechanism of action of PDT involves the photoactivation of a PS, inducing intermolecular triplet-triplet energy transfer to produce highly toxic reactive oxygen species (ROS), particularly singlet oxygen ($^1O_2$). These species are short-lived and highly

toxic to cause cellular damage and subsequent cell death by apoptosis and/or necrosis.[7, 8]

The efficiency of PDT depends on the properties of the photosensitizer. An ideal PS must exhibit: (a) maximum and minimum absorption in its respective red and visible regions; (b) high $^1O_2$ quantum yields; (c) photostability; and (d) high emission capability.[9] The PS should also exhibit no toxicity and high water solubility for better circulation through the blood. Porphyrins and other macrocyclic compounds, such as porphycene, texaphyrin, porphyrazine, chlorin, porphysome[10] and bacteriochlorin have been highly explored as PDT PSs. The high absorption profile in the red region, strong cellular affinity, low dark toxicity, and biocompatibility makes porphyrins potential sensitizers. The sodium salt of hematoporphyrin derivative (HPD), commonly referred to as Photofrin, is currently being used to treat lung and esophageal cancer. Significantly, HPD exhibits strong fluorescence, high tumor uptake, and localizes in the mitochondria.[11, 12] Recently, following second generation PSs, such as benzoporphyrin, that have a more intense long wavelength absorption up to near-IR, third-generation PSs based on selectively targeting subcellular organelles have

received more attention.[13] Multiple targeting subcellular organelles is essential for more efficient PDT action.

ROS has limited intracellular migration range due to its short lifetime.[14] Hence ROS produced by PS is effective only in the subcellular organelle where the PS is localized. Therefore, the subcellular organelles targeted by PS are considered to be a key parameter to elucidate the mechanism of PS-induced cytotoxity against cancer cell. Development of a PS with better efficacy and greater targeting potential is vital.[15] Specific targeting of the PS to multiple subcellular organelles can greatly improve the therapeutic potential of PDT. The problem of multidrug resistance exhibited by cancer cells with respect to chemotherapeutic drugs may also be solved by such a specific target therapy. Modern PDT (third-generation PSs) involves selective targeting of multiple subcellular organelles. Particularly, mitochondria and nucleus have received attention as drug targets since they are crucial regulators of intrinsic and extrinsic apoptosis.[16] Mitochondrial damage affects the energy production of the cells and activates the intrinsic apoptotic pathway mediated by caspases 9 and 3.[17] Mitochondria present in cancer cells are structurally and functionally different from those of normal cells,[18, 19] and exhibit an extensive metabolic reprogramming that leads to

more susceptible mitochondrial perturbations compared to non-immortalized cells.[20-22] DNA breakage has also been reported to induce cellular apoptosis, which proceeds via the intrinsic as well as the extrinsic pathway.[16] Hence, PDT drugs that target both mitochondria and DNA constitute promising therapeutic agents for cancer treatment, and synthesis of PS having multiple targeting capabilities will contribute to the progress in the field of PDT.

High-content cell-based assay (HCA) is very attractive approach to reveal the mechanism of cytotoxicity by PS targeting multiple subcellular organelles against cancer cells. HCA allows simultaneous monitoring of activation/deactivation of intracellular biomarkers.[23] HCA can be used to monitor functionally significant spatial and temporal intracellular dynamics.[24] The concurrent observation of intracellular biomarkers provided by HCA makes it possible to clearly understand PS-induced cytotoxic mechanism through monitoring disruption of subcellular organelle-mediated cellular signaling transductions. In this work, we designed and synthesized a new water-soluble *meso*-substituted porphyrin compound, observed its subcellular localization to investigate whether it targets multiple subcellular organelles, and verified photodynamic efficacy and mechanism to cause

apoptotic cell deaths in the MCF-7 cancer cell line through HCA. A series of caspases involved in intrinsic and extrinsic apoptosis were concurrently monitored at the single cell level by HCA to identify the possible mechanism. In addition, cell death dynamics are discussed based on high-content monitoring of mitochondria disruption, unmaintained homeostasis of cytosolic calcium, and caspase-3 activation under the pathological condition that occurs by light-activated *meso*-substituted porphyrin.

2.1. Results

PDT is especially advantageous as cancer cells can be selectively killed without affecting the adjacent normal cells. The first and second generation PSs used in PDT has some drawbacks which may limit their clinical applications. Recent research is focused on the development of third-generation PSs for selectively targeting subcellular organelles. Targeting mitochondria and nucleus is a good strategy to achieve effective PDT therapy. In this context, a new porphyrin molecule was designed and synthesized and studied its PDT activity.

2.1.1. Synthesis and structural characterization of 5, 10, 15, 20–Tetrakis(Benzo[b]thiophene)porphyrin (BTP)

The novel *meso*-substituted porphyrin with Benzo[b]thiophene (BTP) was synthesized by Lindsey's method **(Scheme 2)**.[25] Typically, BTP was synthesized through one-pot condensation of Benzo[b]thiophene-2-carboxaldehyde with freshly distilled pyrrole in dry CH_2Cl_2 and in the presence of boron trifluoride diethyl etherate ($BF_3 \cdot OEt_2$) as acid catalyst. Then followed by oxidation with *p*-chloranil in air gave BTP with ~10% yield. The compounds were purified by basic alumina column and characterized by using ^1H, ^{13}C NMR, FT-IR and MALDI-TOF analysis.

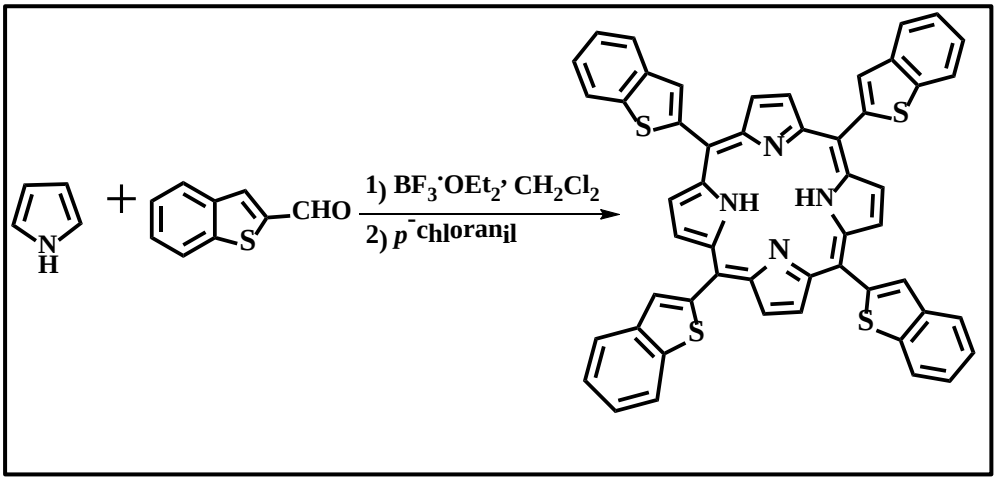

Scheme 2. Synthetic scheme for preparation of BTP

The MALDI-TOF mass spectrum of BTP is showed in **Figure 8.** The m/z value at 839 confirms the formation of BTP molecule.

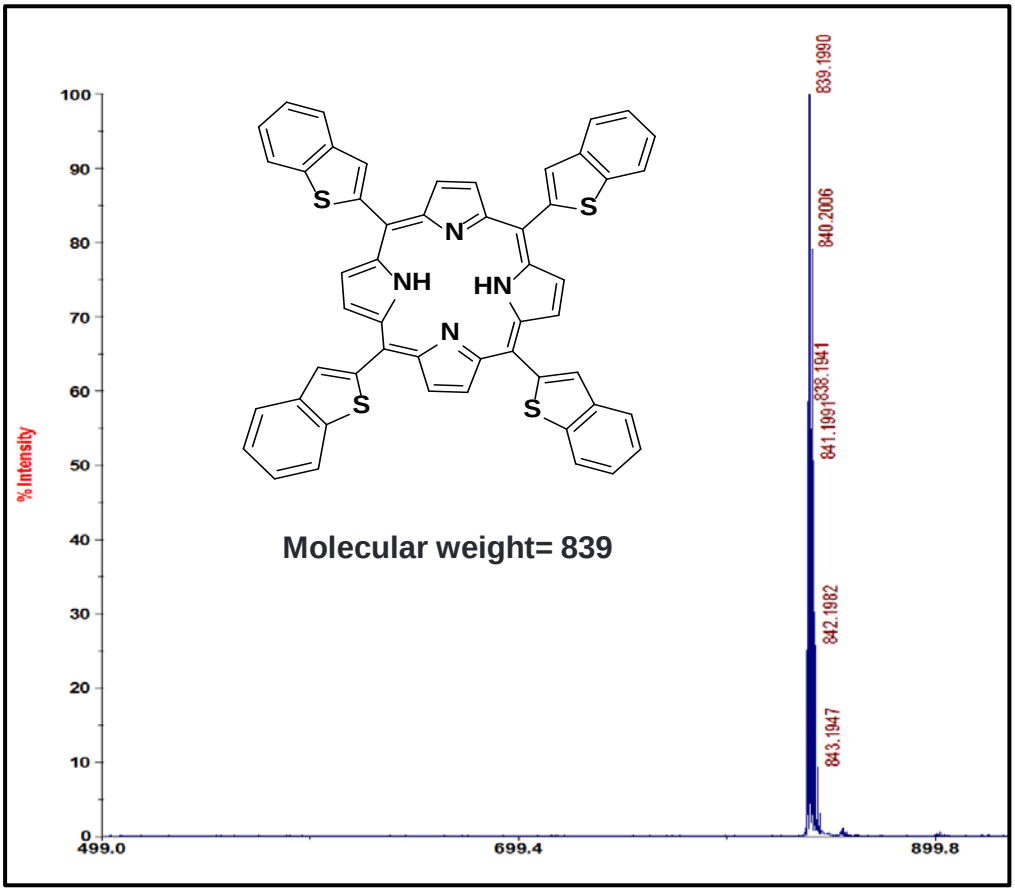

Figure 8. MALDI-TOF spectrum of BTP

Further, structural elucidation was confirmed by ^{1}H NMR spectrum as shown in **Figure 9.** A sharp singlet peak centered at 9.12 and 8.14 ppm corresponds to β-CH protons of pyrrole and thiophene respectively. The phenolic protons are resonated between δ= 7.60 to 8.08 ppm. The inner pyrrolic NH protons were observed at δ= −2.59 ppm.

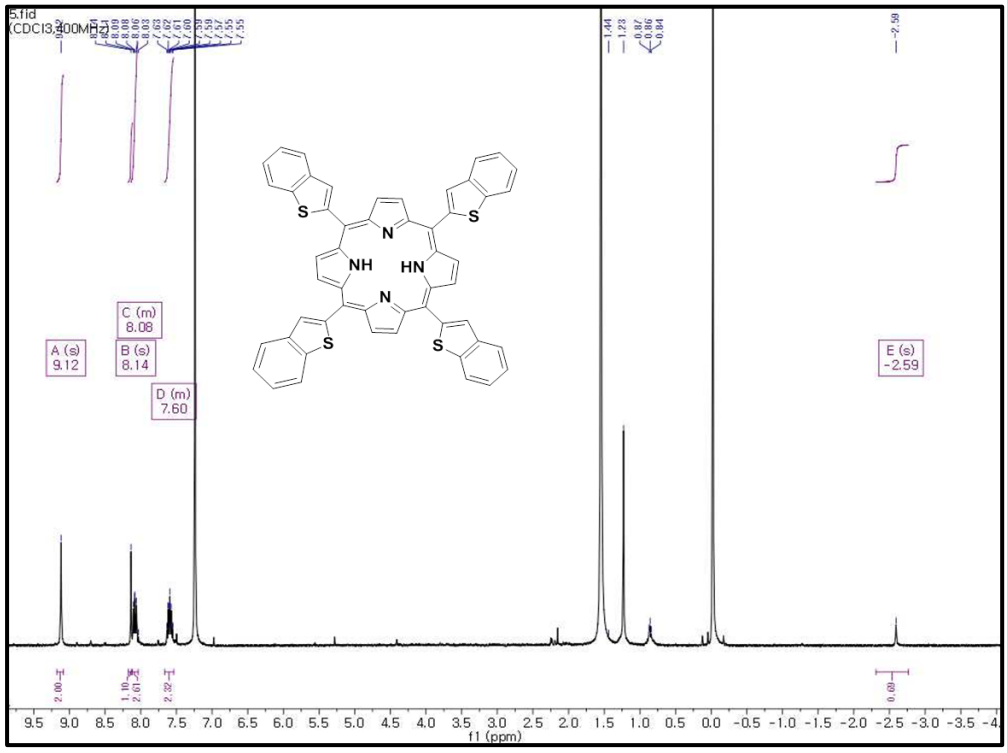

Figure 9. ^{1}H NMR spectrum of BTP

2.1.2. Synthesis and structural characterization of 5, 10, 15, 20–Tetrakis(7-sulfonatobenzo[b]thiophene)porphyrin (SBTP)

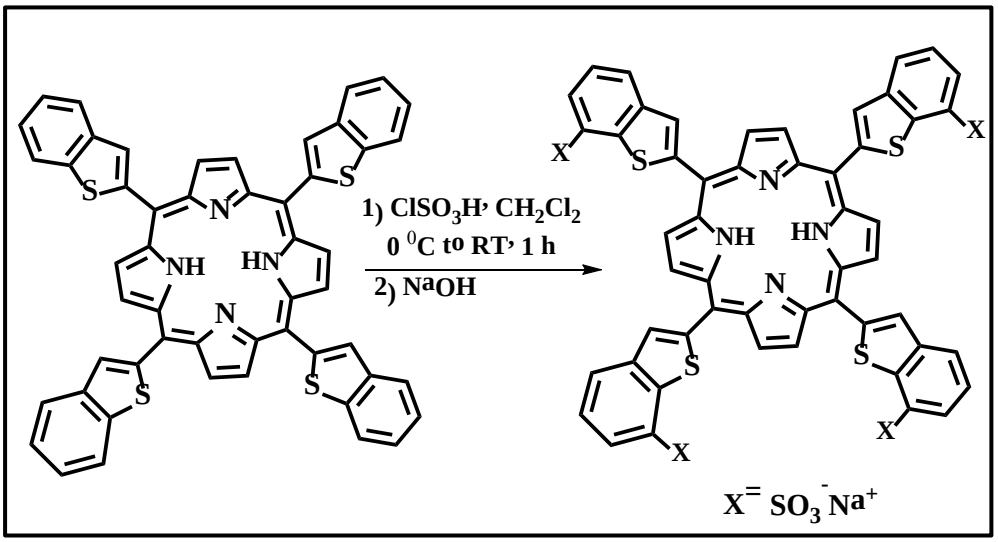

Scheme 3. Synthetic scheme for preparation of SBTP

The water soluble porphyrin 5, 10, 15, 20–Tetrakis(7-sulfonatobenzo[b]thiophene)porphyrin (SBTP) was synthesized from BTP by electrophilic aromatic substitution as shown in **Scheme 3**.[26] Chlorosulfonic acid (CSA) was used as a sulfonating agent. The synthesis of SBTP required optimization of temperature and reaction times. Typically, a required amount of BTP in dry CH_2Cl_2 was added drop-wise to excess of CSA at 0 °C and allowed to stir at room temperature for 1 h. Then excess

acid was quenched and neutralized with NaOH. The precipitate was collected and dissolved in methanol and extracted several times to remove undesired inorganic salts. The crude mixture was precipitated using methanol and acetone.[27] Then the pure compound was obtained after purification by reverse phase column chromatography (C18 silica gel; MeOH: H_2O 50:50) as well as semi-preparative reversed HPLC. SBTP was obtained as a brown solid with 5% yield.

The formation of SBTP was evaluated by using MALDI-TOF mass spectrum **(Figure 10).** The spectrum showed the M+1 peak at 1248.

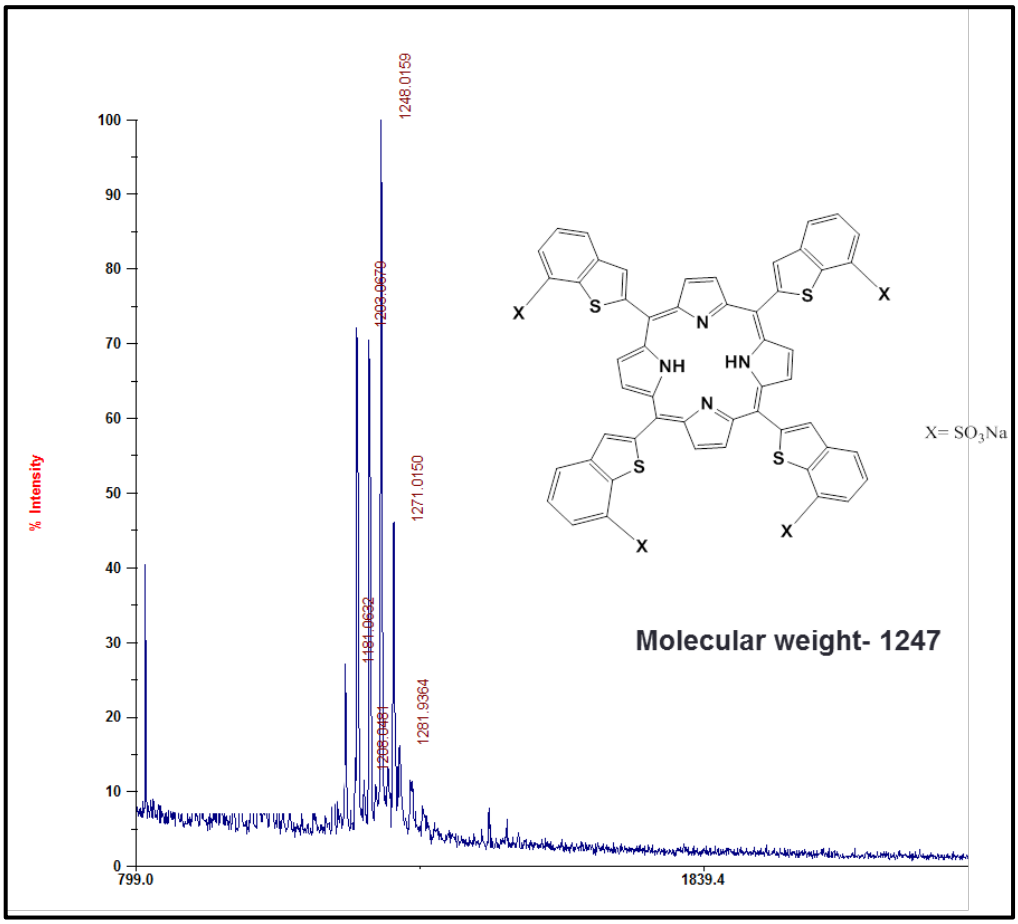

Figure 10. MALDI-TOF spectrum of SBTP

Further, structural elucidation of SBTP was confirmed by ^{1}H NMR spectrum as shown in **Figure 11.** A sharp singlet peak centered at 9.18 and 8.81 ppm corresponds to β-CH protons of pyrrole and thiophene respectively. Three phenolic protons are resonated between δ= 8.20 to 7.59 ppm. The inner pyrrolic NH protons were observed at δ= −2.66 ppm.

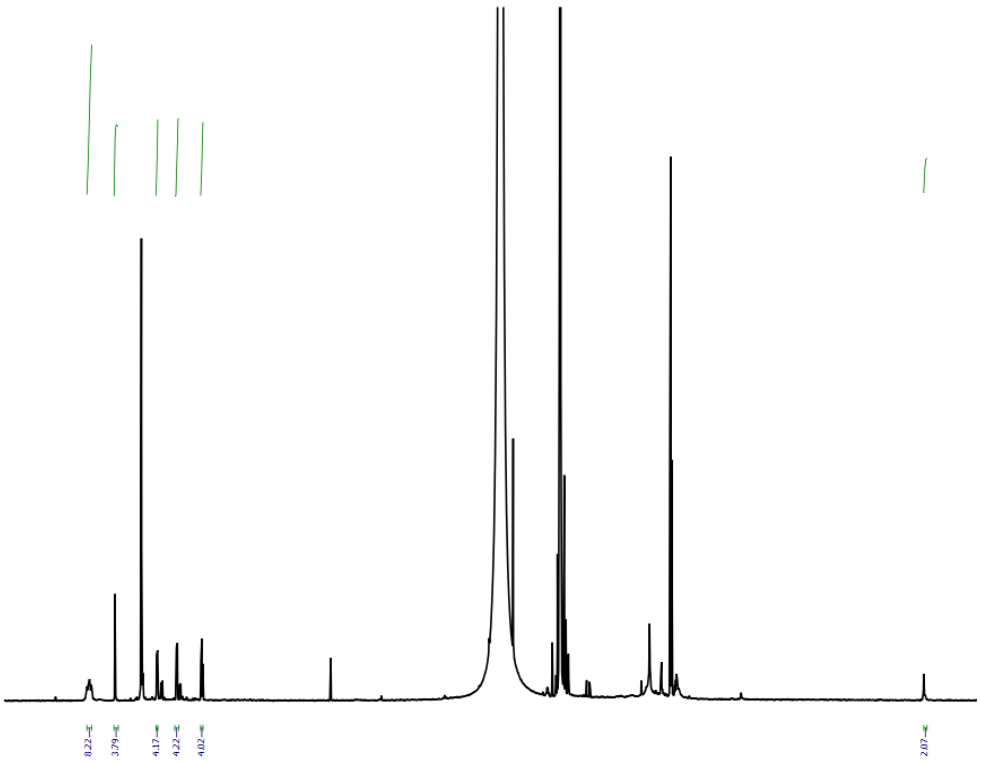

Figure 11. ^{1}H NMR spectrum of SBTP

2.1.3. Photophysical properties of BTP and SBTP

Figure 12a shows the typical porphyrin absorption pattern for **BTP** with a sharp Soret band at 432 nm (ε =430139 $cm^{-1}M^{-1}$) and four Q bands at 525, 561, 600 and 652 nm. The fluorescence spectrum of **BTP** showed emission maxima at 666 nm in toluene (**Figure 12b**). The fluorescence quantum yield was calculated using TPP as the standard (Φ_F= 0.11)[28] and quantum yield of BTP was found to be Φ_F= 0.062 in toluene (Table 1).

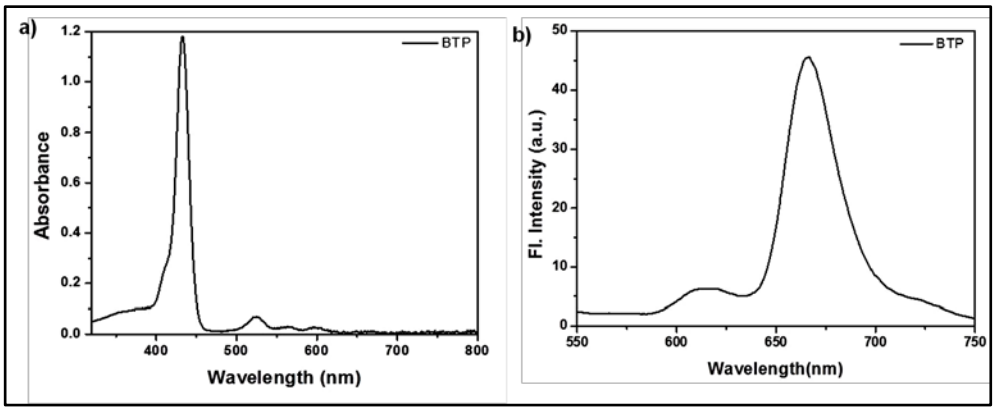

Figure 12. a) Absorption spectrum of BTP in CH_2Cl_2; b) Emission spectrum of BTP in toluene.

Similarly, **SBTP** showed a sharp absorption band (Soret) at 432 nm ($\varepsilon = 432326 cm^{-1}M^{-1}$) and its Q bands at 525, 561, 600 and 652 nm **(Figure 13a)**; and its two emission peaks centered at 615 and 662 nm in methanol **(Figure 13b)**. The relative fluorescence quantum yield of SBTP was measured using $TPPS_4$ as a standard ($\Phi_F = 0.121$) and its value was estimated to be $\Phi_F = 0.058$ **(Table 1)**.

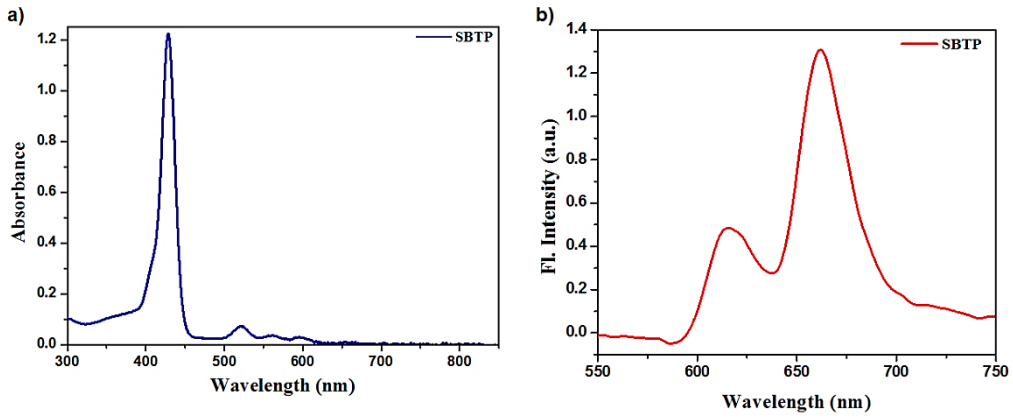

Figure 13. a) Absorption spectrum of SBTP in CH_3OH; b) Emission spectrum of SBTP in CH_3OH.

Table 1

Porphyrin	λ_{abs}	ε ($cm^{-1}M^{-1}$)	Φ_F	Φ ($^1O_2$)
BTP	432	430139	0.062	
SBTP	432	432326	0.058	0.68±0.03

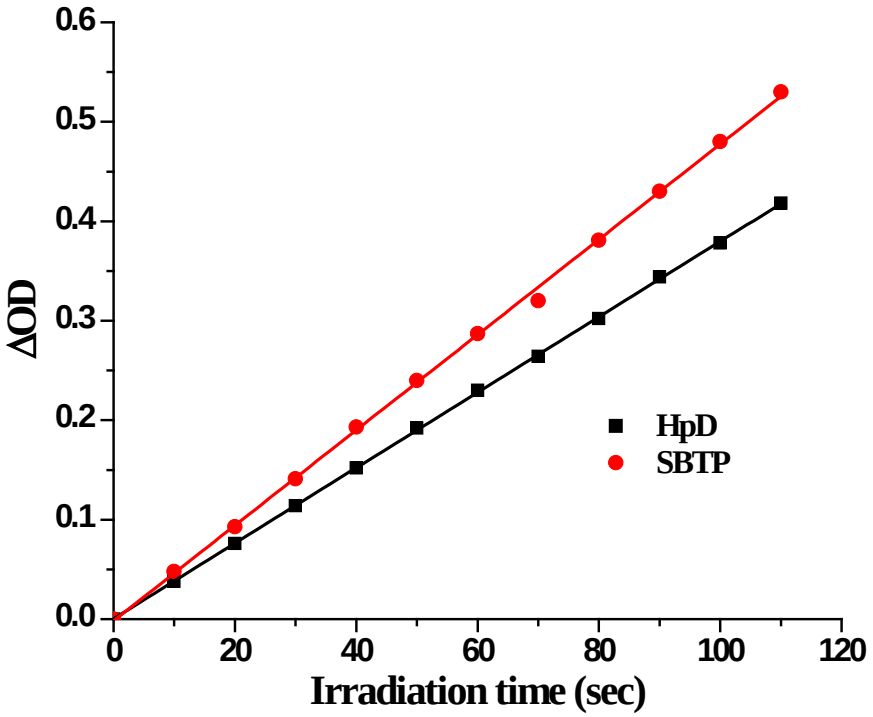

Figure 14. A graph showing change in absorbance of DPBF at 411 nm vs irradiation time in the presence of SBTP vs HpD as control in methanol.

Furthermore, the singlet oxygen quantum yields [$\Phi(^1O_2)$] for SBTP were measured using 1, 3-diphenylisobenzofuran (DPBF) as the singlet oxygen scavenger.[8, 29] SBTP and DPBF were irradiated with 660 nm laser light for a time interval between 0 to 110 seconds. A change in absorption and a decrease in absorbance for DPBF were monitored at 410 nm. Hematoporphyrin (HpD) was used as the standard ($\Phi(^1O_2)$=0.60 in methanol) to measure the relative singlet oxygen quantum yield. The quantum yields were calculated from the slope of the graph by plotting the change in optical density against irradiation time **(Figure 14)**, and it was calculated as 0.68±0.03 in methanol. The detailed photophysical properties of SBTP are presented in Table 1.

2.1.4. Cytotoxicity and photocytotoxicity of SBTP

Cytotoxicity and photocytotoxicity of **SBTP** were evaluated on human breast cancer cell line (MCF-7) by MTT assay.

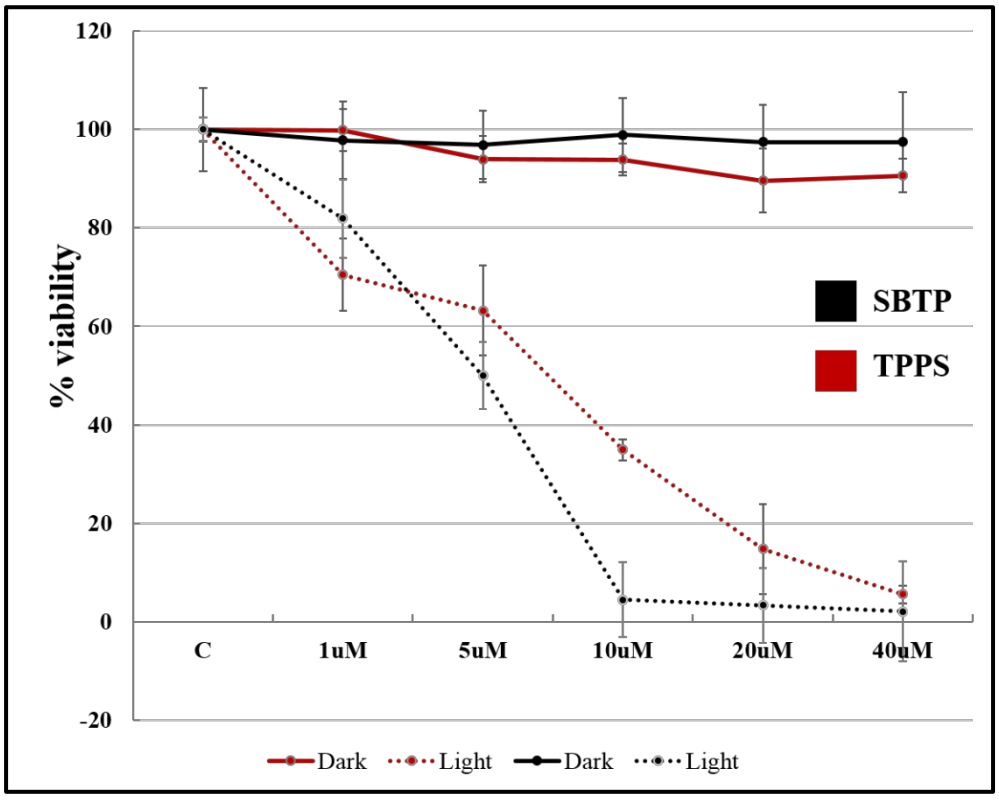

Figure 15. Cytotoxicity assay for SBTP and $TPPS_4$ performed on the MCF-7 breast cancer cell line under light and dark conditions. SBTP shows significant cell death in the presence of light, and shows negligible cytotoxicity under dark conditions. The IC_{50} value for SBTP was determined to be 5 μM.

Figure 15 shows the result of the MTT assay performed at varying concentrations (0 to 40 μM) of SBTP and $TPPS_4$ under dark and light conditions. Interestingly, SBTP under dark condition did not show any cytotoxic effect up to a concentration of 40 μM. However, under light conditions (660 nm, 50 mW, 30 min) it showed decreased cell viability and IC_{50} value for SBTP was determined as 5 μM. PDT activity of SBTP was evaluated with the control. The control experiments were performed with $TPPS_4$. The MTT assay results revealed the IC_{50} of $TPPS_4$ to be 11.76 μM. This result indicates that SBTP is a more effective PS compared to $TPPS_4$.

2.1.5. Subcellular localization of SBTP

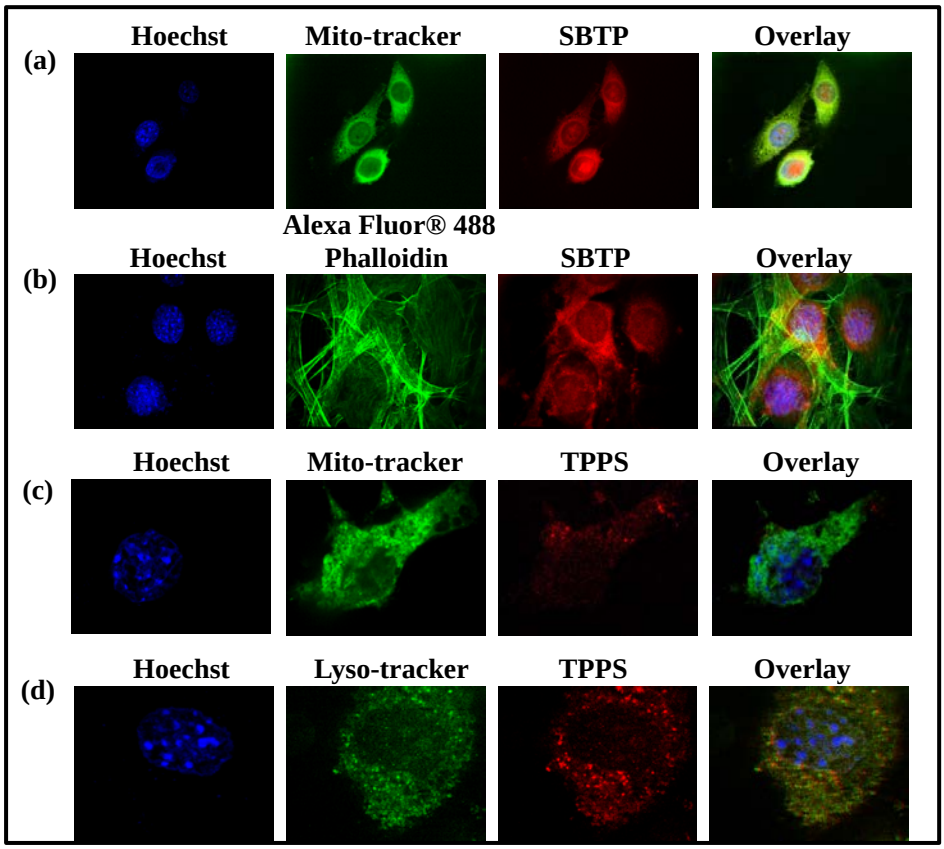

Figure 16. Subcellular localization of SBTP. Confocal fluorescence microscopic images of MCF-7 cells preincubated with 10 μM of SBTP for 4 h: (i) a) Hoechst staining; b) Mitotracker green staining; c) SBTP; and d) merged images of a-c. (ii) a) Hoechst staining; b) Alexa Flour 488 phalloidin staining; c) SBTP; and d) merged images of a-c; (iii) a) Hoechst staining; b) Mitotracker green staining; c) $TPPS_4$; and d) merged images of a-c; (iv) a) Hoechst staining; b) Mitotracker green staining; c) $TPPS_4$; and d) merged images of a-c.

Confocal microscopy and organelle-specific probes were used to observe the subcellular localization of SBTP. Localization assay results show that **SBTP** was localized mainly in the mitochondria with some observed in the nucleus. The fluorescent images of **SBTP** and mitotracker green on MCF-7 cells were almost overlapped. This demonstrates large amount localization in mitochondria **(Figure 16a)**. Also, we observed co-localization of **SBTP** in the nucleus from the merged images of SBTP and Hoechst dye **(Figure 16b)**. No localization was observed in the F-actin filament (Alexa Fluor® 488 Phalloidin) and as well as in lysosomes (data not shown). A control experiment was performed with $TPPS_4$. **Figure 16c** and d shows that anionic $TPPS_4$ mainly localized in the lysosome.[30] This result revealed that anionic porphyrin with different substitutions on the porphyrin ring help in selective accumulation in mitochondria.

2.1.6. Cellular uptake property of SBTP

Cellular uptake by cancer cells is an important property of PSs. The cellular uptake in MCF-7 cells was monitored through intracellular fluorescence of SBTP and visualized by fluorescence microscope. A significant amount of red fluorescence of SBTP was observed within 20 minutes after treatment **(Figure 17).** The cellular fluorescence intensity increased with the increase in incubation period.

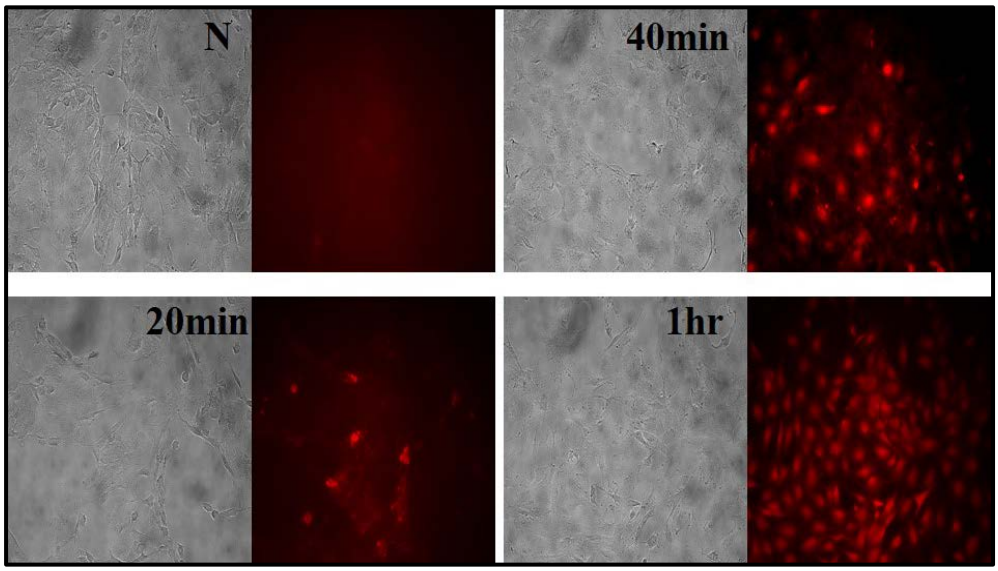

Figure 17. Fluorescence microscopic images show time-dependent cellular accumulation of SBTP in MCF-7 cells.

Additionally, the uptake of SBTP by MCF-7 cells was investigated by FACS analysis.[31] **Figure 18** shows the FACS analysis of MCF-7 cells treated with SBTP at 20, 40 and 60 min after treatment. After an incubation of 1 hour, the fluorescence intensity of SBTP was significantly increased three folds compared to that of control cells. The data show that fluorescence intensity of SBTP was observed within the first 20 minutes suggesting a rapid cellular uptake by MCF-7 cells.

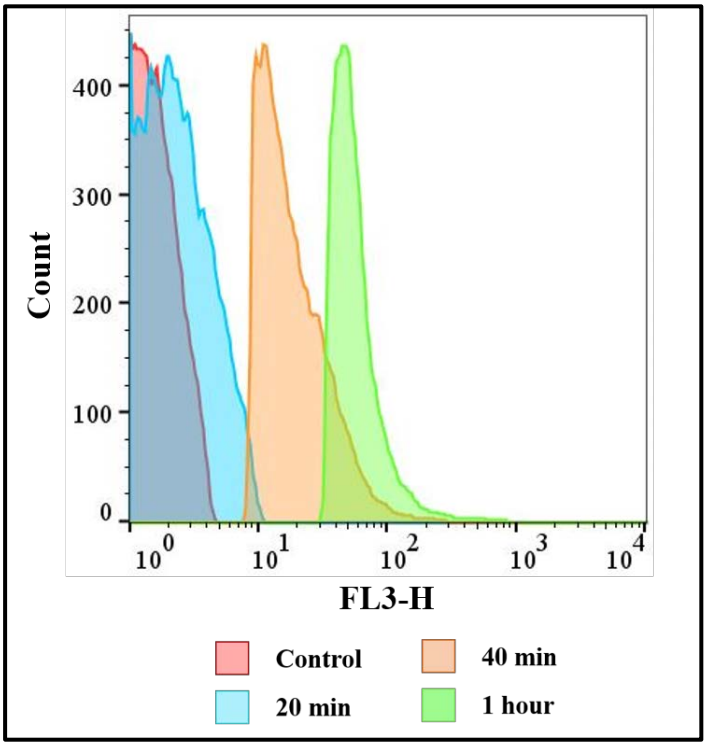

Figure 18. FACS analyses of MCF-7 cells treated with SBTP showing the fluorescence associated to the cells was detected at 20, 40, and 60 min after incubation.

2.1.7. Intracellular ROS generation of SBTP under photodynamic action.

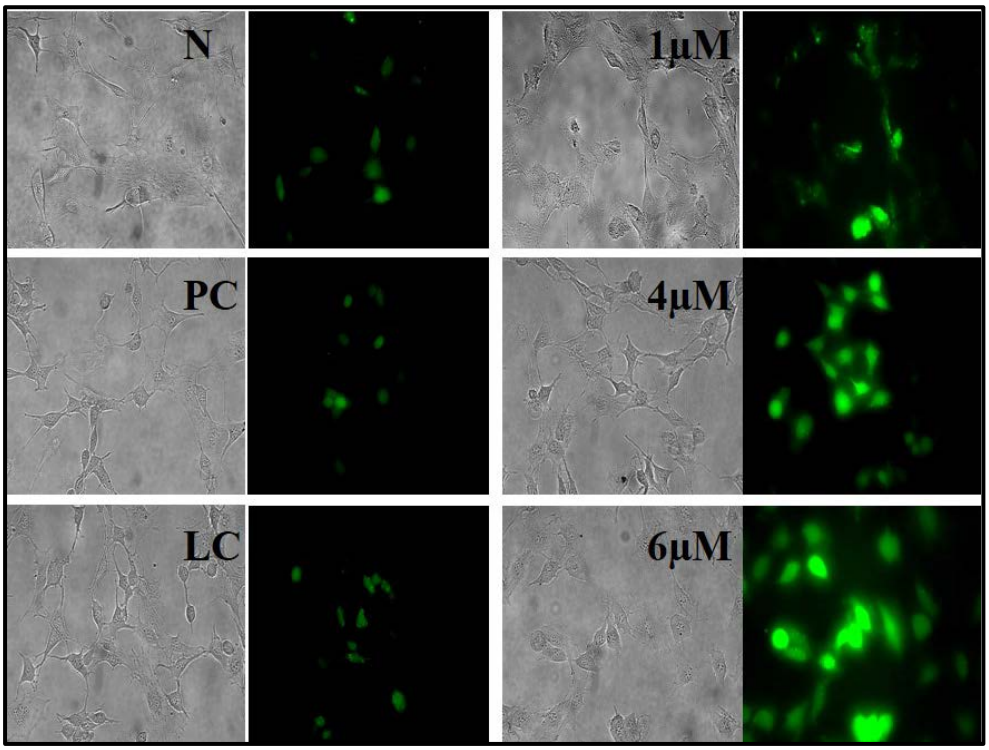

Figure 19. Green fluorescent microscopic images showing concentration-dependent ROS generation in MCF-7 cells after photodynamic treatment by SBTP and detected by incubation with ROS indicator 2′,7′-Dichlorofluorescin diacetate.

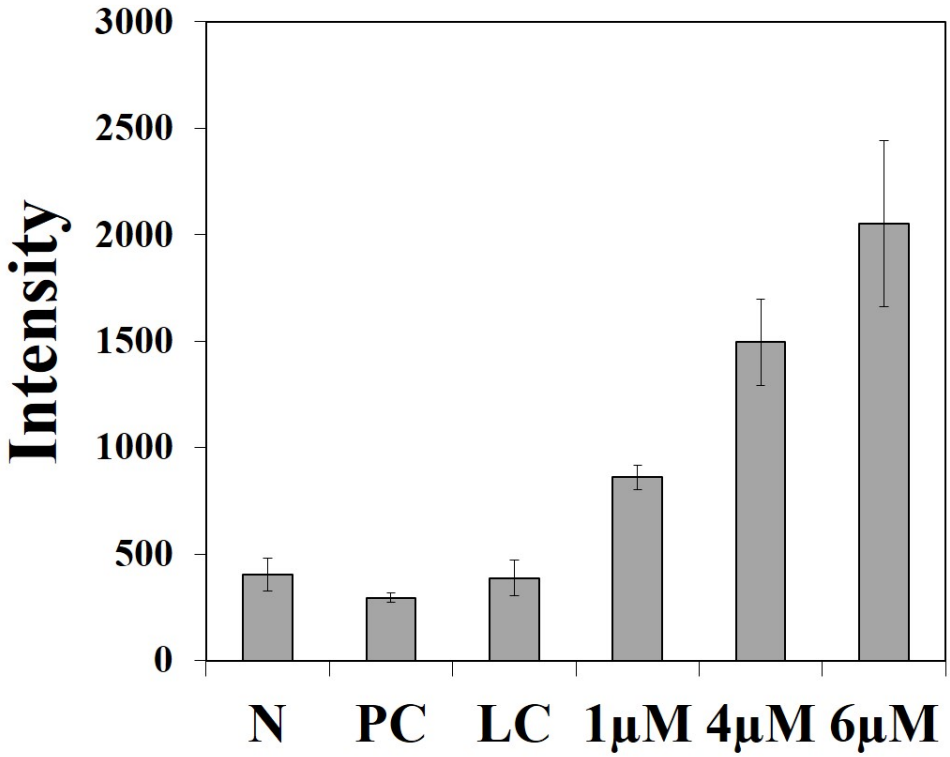

Figure 20. Bar graphs represent the mean ± SD fluorescent intensity values of triplicate treatment groups to analyze the ROS production by SBTP treated MCF-7 cells. Error bars represent the standard deviations of three independent experiments.

The production of ROS in cells by a PS is crucial for photodynamic activity. The intracellular ROS generation by SBTP in MCF-7 cells was estimated by using a cell permeable fluorescent-probe 2'-7'- dicholofluorescein-diacetate (DCFDA). **Figure 19** shows green fluorescent images suggesting intracellular ROS generation in MCF-7 cells by SBTP after PDT. **Figure 20** shows normalized fluorescence intensity increases in concentration-dependent manner.

2.1.8. High-content cell death dynamics.

Figure 21 represents the cell death dynamics of MCF-7 cells under SBTP and PDT treatments. Mitochondrial membrane disruption, increase of cytosolic calcium amount, and caspase-3 formation were concurrently monitored as a function of SBTP concentration. A sharp reduction of fluorescence intensity of the calcein-AM accumulated on mitochondria was observed from 1 μM of SBTP due to damage that occurred on the mitochondria by SBTP-induced ROS. The fluorescence intensity of the calcein-AM was almost saturated to the lowest value from 3 μM of SBTP. On the other hand, the amount of cytosolic calcium showed a steady increase as the concentration of SBTP increased. Compared with calcein-

AM and cytosolic calcium, the formation of caspase-3 was much less influenced with SBTP treatment. However caspase-3 levels increased after 3 μM SBTP treatment, and the maximum values were found for the 5 μM SBTP treatment groups.

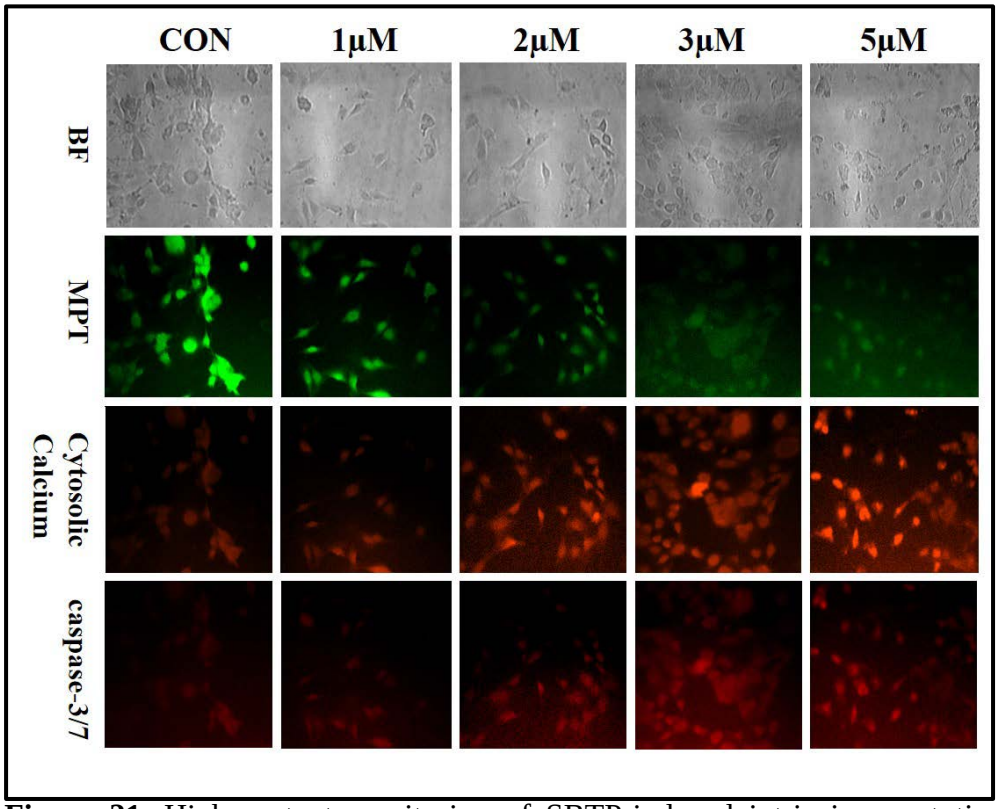

Figure 21. High-content monitoring of SBTP-induced intrinsic apoptotic cell death after PDT. MCF-7 cells were treated with 1, 2, 3, and 5 μM SBTP. The green (upper figure) and red fluorescent images (middle and bottom figures) correspond to cellular images of MPT, intracellular Ca^{2+}, and caspase-3.

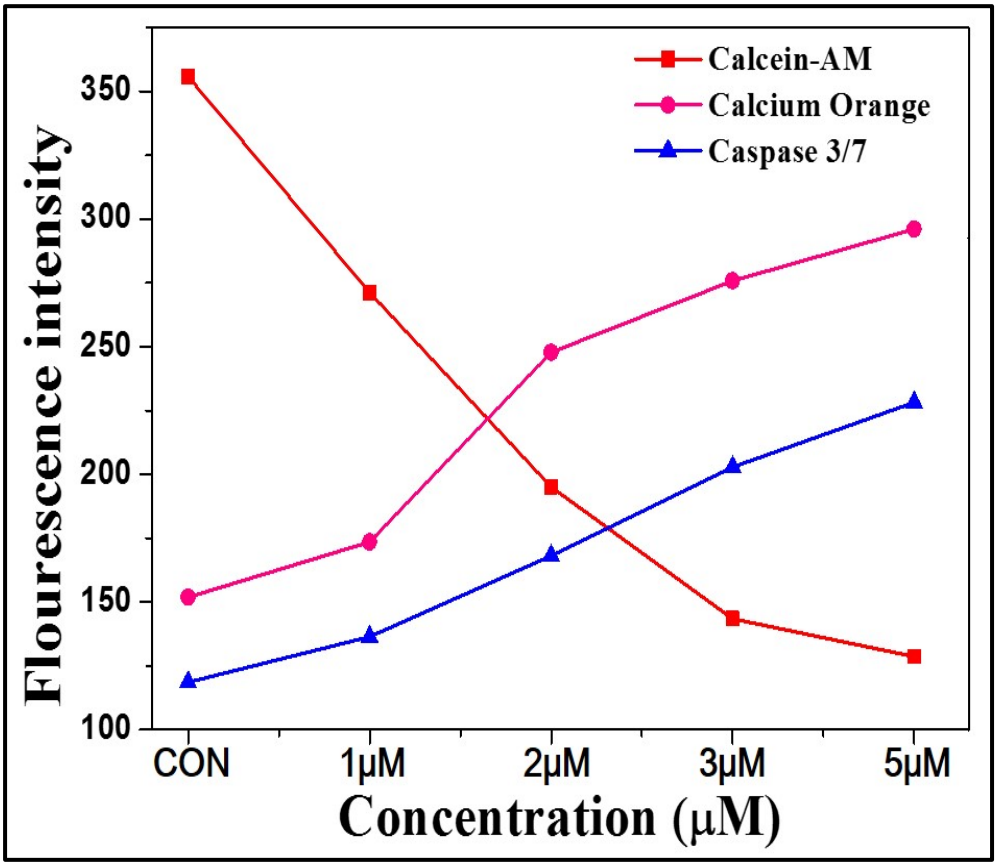

Figure 22. Graph showing the normalized cellular fluorescence intensities of Calcein-AM, Calcium orange and Caspase 3/7 were plotted as a function of concentrations.

2.1.9. Studies on intrinsic and extrinsic apoptotic pathways

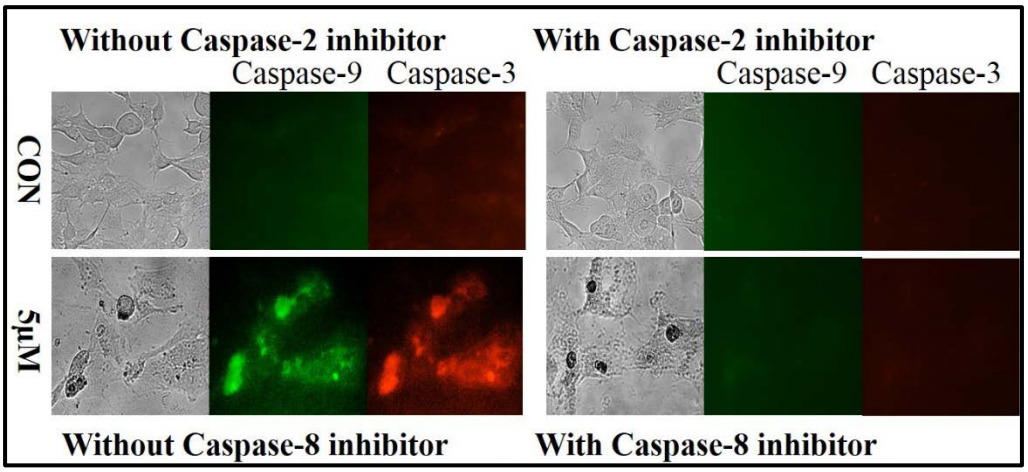

Figure 23. Fluorescent microscopic images showing caspase-9 and caspase-3 activation after PDT treatment of SBTP with and without caspase-2 inhibitor. Fluorescent images were taken at 523 nm (caspase-9) or 617 nm (caspase-3). MCF-7 cells were pre-incubated with fluorigenic caspase-9 [(Ac-LEHD)2-Rh110] and caspase-3 [(z-DEVD)2-Magic Red] substrates with or without the presence of caspase-2 inhibitor, and were analyzed through cellular imaging cytometry.

Light-activation of SBTP triggered caspase-9 and caspase-3 activation in MCF-7 cells **(Figure 23).** Compared to the control, caspase-9 and caspase-3 activation were clearly observed by the treatment of 5 μM SBTP. A caspase-

2 inhibitor, Z-VDVAD-FMK, was used to demonstrate the involvement of caspases in SBTP-caused apoptosis.[32] SBTP-induced caspase-9 and caspase-3 activation were remarkably diminished by the pretreatment with caspase-2 inhibitor **(Figure 23).** This phenomenon suggests that caspase-9-mediated signaling occurs in SBTP induced apoptosis. Caspase-9 is closely related to the intrinsic apoptotic pathway.

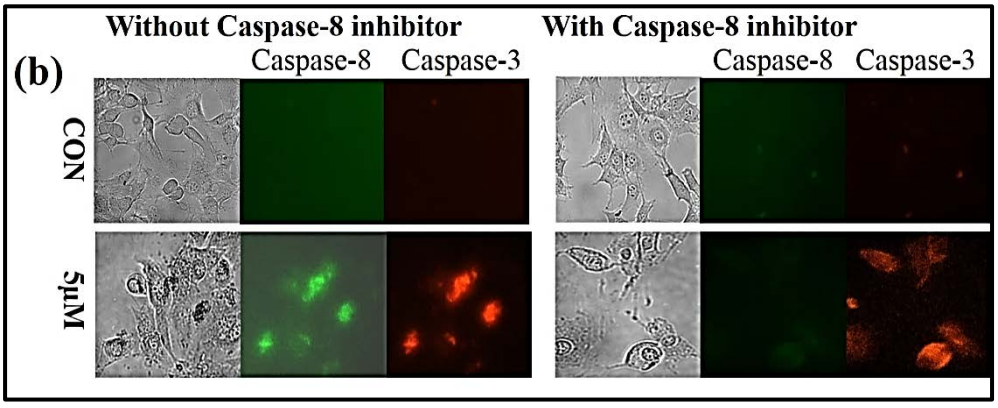

Figure 24. Fluorescent microscopic images of caspase-8 and caspase-3 activation after PDT treatment by SBTP with and without caspase-8 inhibitor. Caspase-8 fluorescent images were taken at 523 nm, and caspase-3 fluorescent images were taken at 617 nm. MCF-7 cells were pre-incubated with fluorogenic caspase-8 [(z-IETD)2-Rh110] and caspase-3 [(z-DEVD)2-Magic Red] substrates with and without caspase-8 inhibitor, and were analyzed through cellular imaging cytometry.

Caspase-8 and caspase-3 activation assays were performed to investigate the possibility of SBTP-caused apoptosis through the extrinsic apoptotic pathway **(Figure 24).** As shown in **Figure 24**, caspase-8 and caspase-3 were activated by the treatment of 6 μM SBTP. A specific caspase-8 inhibitor, Z-IETD-FMK, was used to confirm the occurrence of SBTP-induced extrinsic apoptosis. Pretreatment with caspase-8 inhibitor significantly eliminated the formation of caspase-8. These results indicate that SBTP-induced apoptosis occurred via the extrinsic pathway, as well as the intrinsic pathway.

2.20. DNA fragmentation assay

Figure 25 represents DNA fragmentation of MCF-7 cells induced by SBTP localized in their nucleus. Compared with the genomic DNA band pattern of the control group, a 5 μM dose of SBTP caused significant damage to DNA as evidenced by the presence of several small DNA fragments **(Figure 25b).** The localization assay clearly showed the accumulation of SBTP in the nucleus. This result suggests the possibility of multi-target PDT action by SBTP because ROS produced by SBTP can cause damage to DNA, as well as mitochondria simultaneously.

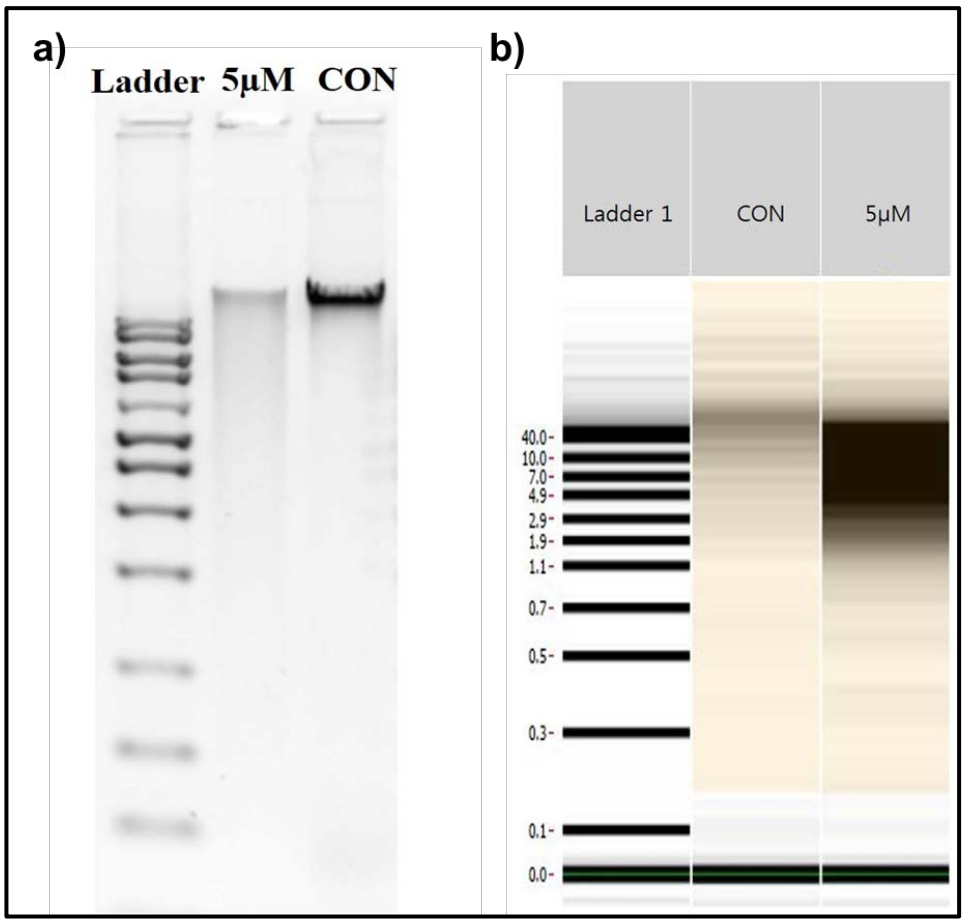

Figure 25. Nucleus-mediated apoptotic cell death confirmation by DNA ladder assay. a) Gel image to represent genomic DNA fragmentation pattern in MCF-7 cells after photodynamic treatment with SBTP. Lane 1: DNA ladder; lane 2: MCF-7 cell treated SBTP (5 μM); and Lane 3: control cells. b) Gel-like images showing DNA fragmentation of SBTP after PDT was analyzed by using Labchip GX. Lane 1: DNA ladder marker; lane 2: control cells; and lane 3: MCF-7 cell treated SBTP (5 μM).

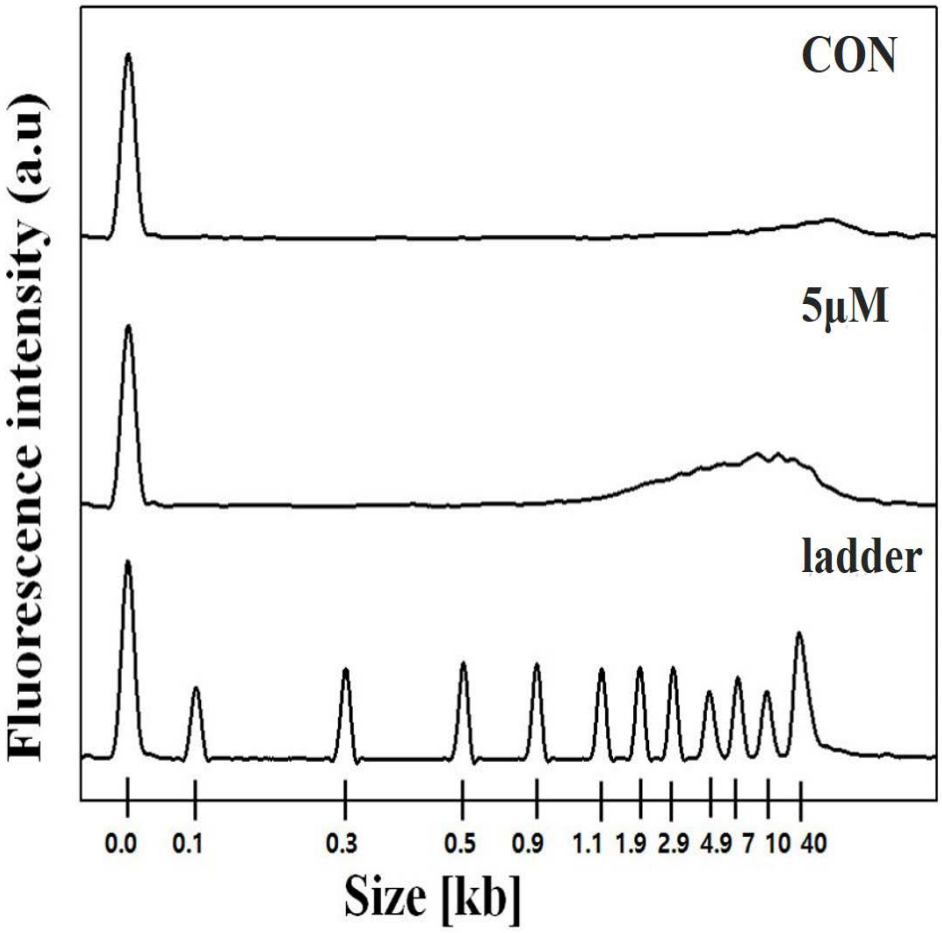

Figure 26. An electropherogram overlay of DNAs that correspond to the control, treatment of SBTP, and DNA ladder.

2.2.0. Discussion

Water soluble 5, 10, 15, 20–Tetrakis(7-sulfonatobenzo[b]thiophene)porphyrin SBTP showed selective targeting of mitochondria and nucleus and effectively mediated apoptotic cell death in MCF-7 cells. It was speculated that *meso* substituted Benzo [b] thiophene was responsible for selective targeting in mitochondria and nucleus. Many Benzo[*b*]thiophene derived compounds are used as antitumor agents. For example, drugs like Raloxifene had demonstrated mitochondria-mediated apoptotic cell death in human endometrial carcinoma cells.[33] Similarly, Benzo[b]thiophenesulphonamide 1,1-dioxide (BTS) derivatives are known to induce ROS and kill cancer cells by apoptosis. BTS undergoes a typical apoptotic process that comprises mitochondrial dysfunction, internucleosomal DNA degradation, caspase activation, cell shrinkage, phosphatidylserine translocation to the cell surface, and chromatin condensation.[34]

In the present work, chlorosulfonic acid (CSA) has been used to synthesize SBTP from BTP. CSA is a versatile reagent and has been widely used as a chlorosulfonating and sulfonating agent with aromatic, aliphatic, and heterocyclic compounds.[35, 36] It has also been used previously to synthesize

chlorosulfonic derivatives of porphyrins and corroles in high yields. Chlorosulfonic acid used in this work allowed much milder reaction conditions (0-25°C) compared to other sulfonating agents that require >100°C.[37] In addition, it undergoes substitution reaction preferably at the aryl position, with the other positions are substituted with less selectivity. In accordance with this, when BTP reacted with excess CSA under cold conditions, it produced SBTP in high yields, and other inorganic salts were formed in minor quantities. The electrophilic aromatic substitution took place at the C7-position of Benzo[*b*]thiophene due to the high reactivity of the thiophene ring. The MALDI-TOF and ^{1}H NMR spectra confirmed the formation of SBTP.

The photophysical properties of porphyrins make them suitable for use in PDT as well as in tumor imaging.[7, 38] For therapeutic applications PSs should have absorption peaks around 630 to 850 nm due to low human tissue permeability to light below 600 nm. Our results confirmed that BTP and SBTP showed enhanced photophysical properties due to Benzo[*b*]thiophene substitution at the *meso* position. Both the compounds demonstrated characteristic porphyrin absorptions Soret and Q bands due to π–π*.[39] Further, they had longest absorption in the red spectral region and

emitted at 666 nm. Thus, understanding the importance of red and far-red spectral region as the phototherapeutic window, the photophysical properties of SBTP allowed it to absorb the light efficiently in the red region to perform better PDT action.

Subcellular localization of the PS is crucial in determining the fate of cells and cell death mechanism.[40, 41] Previous studies revealed that PSs with sulfonate or carboxyl groups were localized mainly in the cytoplasm and translocated to the nucleus upon light irradiation.[42] However, from the localization experiments we observed that SBTP accumulated mainly in mitochondria and to some extent in the nucleus. Although the mechanism of selective localization of SBTP is not completely understood, we assume that Benzo[*b*]thiophene substitution may play the key role for selective accumulation in mitochondria. To understand whether a negatively charged porphyrin can accumulate in mitochondria, we performed control experiments with an anionic porphyrin ($TPPS_4$). It revealed that $TPPS_4$ primarily localized in lysosome and it further confirmed no localization in mitochondria. This is in agreement with previously published results.[30] B. C. Wilson et al. had studied subcellular localization of negatively charged photofrin and found that Photofrin bound to mitochondria and upon light

irradiation induced inactivation of specific mitochondrial enzymes.[12] Other studies also suggested that Photofrin consistently binds to the inner mitochondrial membrane, specifically to cardiolipins.[43] Affinity towards mitochondria membranes also depends on the substitution of porphyrin ring and can make the molecule very lipophilic.[44, 45] Therefore, we speculated that the substitution of the Benzo[b]thiophene moiety at the porphyrin ring would be crucial in targeting mitochondria and this was verified by the subcellular localization images.

Subcellular localization results showed that the negatively charged SBTP localized in the nucleus. This phenomenon is contradictory since negatively charged porphyrins are believed to be repelled by the negatively charged nucleus due to electrostatic repulsions. However, recent studies have demonstrated the binding of anionic porphyrins to DNA based on π-π interaction.[46, 47] π-π interaction may provide anionic porphyrins with a possibility of interacting with the nucleus if they overcome the electrostatic repulsion between anionic porphyrin and the nucleus. Interestingly, Purrello et al reported the interaction between DNA and anionic nido-carboranyl porphyrins,[48] It was suggested that under physiological conditions the protonation of porphyrin's inner core leads to a reduction in electrostatic

repulsions and a non-covalent interaction caused by a chirality match. Based on this phenomenon, the protonation of the inner core of SBTP can lead to the reduction in the electrostatic interaction between the SBTP and the nucleus, thus making it feasible for localization in the nucleus. Also, SBTP showed high level of cellular uptake within a very short time range that may be crucial for its use as a potential PS from the therapeutic aspect.

Cancer cells can undergo cell death via apoptosis or necrosis after PDT. Apoptosis is the most common mode of cell death. Cellular apoptosis is regulated by various extracellular and intracellular signals. Previous studies suggest that PSs localized in the mitochondria are able to induce apoptotic cell death very rapidly.[41] In normal cellular conditions, mitochondria play the role of buffering Ca^{2+} concentration for the homeostasis of cytosolic Ca^{2+}levels. During the pathological conditions, an enlarged amount of cytosolic Ca^{2+} disrupts the mitochondrial potential and leads to MPT.[49] The Mitochondrial Permeability Transition (MPT) is defined as an increase in the permeability of molecules into mitochondrial membranes. Mitochondria maintain a particular mitochondrial membrane potential formed through the transfer of protons from the mitochondrial matrix to the intermembrane space by mitochondrial complexes. The reduction of the mitochondrial

membrane potential is directly related to MPT. Induction of MPT can lead to mitochondrial swelling and cell death through apoptosis. Therefore, we used MPT to measure mitochondrial membrane disruption.

Intracellular translocation of cytochrome c from mitochondria to cytosol due to the disruption of mitochondrial membrane upon PDT action is observed in cancer cells. In this work, apoptotic cell death dynamics were studied by monitoring cytosolic Ca^{2+}, MPT, and caspase-3/7 simultaneously at the single-cell level through a hypermulticolor HCA.[32, 50] MPT causes an increase in the cytosolic Ca^{2+} concentrations, which then leads to the activation of caspase-3. As revealed from the localization assay, SBTP on mitochondria upon PDT action produces ROS which causes severe damage to mitochondria. SBTP can disrupt mitochondrial membrane immediately upon light activation that leads to a remarkable decrease of calcein-AM fluorescence intensity even at a lower SBTP concentration compared to the rates of increase in cytosolic Ca^{2+} contents and caspase-3 activation.

An interesting result in this work was that the extrinsic pathways, as well as the intrinsic pathway, were activated in SBTP PDT-induced apoptosis. The intrinsic apoptosis pathway involves the translocation of cytochrome C mitochondria to cytosol. The cytosolic cyt c causes the activation of

caspase-9 which combines with apaf-1 to form apoptosome that activates caspase-3 to induce apoptosis. Extrinsic pathways start from fas receptor activation those results in the cleavage of procaspase-8 to produce active caspase-8. Activation of caspase-8 results in the activation of caspase-3 and caspase-7, leading to apoptosis. In order to confirm that roles of caspases in SBTP-induced cell death, we used specific caspase inhibitors to assess their roles in cellular apoptosis. Inhibition of caspase-2 blocked the activation of caspases -9 and -3 thus proving the role of SBTP in inducing intrinsic apoptosis. However caspase-8 inhibition could not completely block the activation of caspase-3, the reason may be the simultaneous operation of the intrinsic pathway to generate activated caspase-3.

The localization of SBTP in mitochondria induced intrinsic apoptosis that lead to cytochrome c release from mitochondria with subsequent activation of the caspases -9 and -3. The extrinsic pathway involves the activation of caspase-8 and its downstream effector caspase-3. In consideration of the co-localization of SBTP in mitochondria and nucleus, the activation of extrinsic apoptotic pathway is thought to arise from DNA damage by ROS produced due to the PDT action of SBTP localized in the nucleus. The SBTP PDT-induced genomic DNA fragmentation in MCF-7 cells was clearly visualized

(Figure 8). DNA damage is an obvious cause of apoptosis induction in order to arrest cellular activation and remove the damaged cells. Double stranded breaks (DSB) resulting from impaired replication machinery are crucial mediators of downstream apoptosis signaling cascade, as determined by experiments with DNA repair deficient mutant[51, 52] Activation of the death receptors of the extrinsic apoptotic pathway is the general mechanism of DNA damage-induced cell death along with the induction of the intrinsic apoptotic signaling.[52] Hence, DNA is the prime target in anticancer drug therapy. The activation of caspase-8-mediated extrinsic apoptosis by SBTP PDT action may be a consequence of DNA damage. The concomitant activation of the extrinsic apoptotic pathway was previously observed.[53-56]

2.3.0. Conclusions

The synthesis of water-soluble porphyrin with Benzo[b]thiophene moiety at the *meso*-position selectively targeted mitochondria and DNA. Due to this selective localization, SBTP induced intrinsic and extrinsic apoptotic cell death by the PDT action. A photosensitizer with such low working

concentrations and multi-targeting potential may prove to be a useful in cancer therapy.

2.4.0. Materials and methods

2.4.1. General methods

All chemicals and reagents for the synthesis of porphyrins were purchased from Sigma-Aldrich and Dae-Jung chemicals and metals co. Ltd., South Korea. Solvents and pyrolle for reraction were distilled prior to use. All the reactions were conducted at inert atmosphere. The NMR spectrum was recorded in $CDCl_3$ and DMSO-d6 at 25 ^{0}C on a 400 and 500 MHz Bruker Avance FT-NMR spectrometer and the TMS was used as an internal standard. IR spectra were recorded in the range of 4,000-400 cm^{-1} with a JASCO, FT/IR-4200 spectrometer using KBr pellets. Elemental analyses (C, H, N, S) were performed on CE Instruments' EA 1110. MALDI-TOF mass spectrum was recorded using a MALDI TOF-TOF 5800 System. Thin layer chromatography (TLC) was performed on silica gel Merck TLC Silica gel 60 F_{254} plates and visualized with UV (λmax 254 or 365 nm). UV−vis spectra were recorded on Evolution 60, Thermo Scientific

spectrophotometer. Fluorescence spectra were recorded on Jasco- FP 6500 spectrofluorometer.

Singlet oxygen quantum yield was measured by a steady-state method using 1,3-diphenylisobenzofuran (DPBF) as the scavenger of singlet oxygen and HpD as the reference. Quantum yield for singlet oxygen generation of SBTP in methanol was determined by monitoring the photooxidation of DPBF during the formation of singlet oxygen using an absorption spectrometer. Concentration of the photosensitizer was adjusted with an optical density of 0.02−0.03 at the irradiation wavelength (660 nm) to minimize the possibility of singlet oxygen quenching at higher concentrations. The photooxidation of DPBF was monitored with an interval of 10 to 110 seconds. The following equation was used to calculate the singlet oxygen quantum yield of the sensitizer with respect to the reference.

$$\Phi\ (^1O_2)^{comp} = \Phi(^1O_2)^{ref}\ \frac{m^{comp}}{m^{ref}}\ \frac{F^{ref}}{F^{comp}}$$

$\Phi\ (^1O_2)$ is the quantum yield of singlet oxygen. Superscripts “comp”and “ref” represents SBTP and HpD, respectively. M is the slope of a plot of difference in change in absorbance of DPBF (at 411 nm) with the irradiation

time. F is the absorption correction factor, which is given by $F = 1 - 10^{-OD}$ (OD at the irradiation wavelength). Based on the obtained parameter values above, it was calculated that SBTP exhibited Φ ($^1O_2$) = 0.68 in methanol.

2.4.2. Synthesis of 5, 10, 15, 20 – Tetrakis(benzo[b]thiophene) porphyrin (BTP).

Synthesis of 5, 10, 15, 20–Tetrakis (benzo[b]thiophene) porphyrin involved the condensation between Benzo[*b*]thiophene-2-carboxaldehyde (1 g, 6.2 mmol) and freshly distilled pyrrole (0.43 mL, 6.2 mmol) in dry dichloromethane (620 mL) taken in a 1 liter round-bottomed flask kept under nitrogen atmosphere for 15 min. Then, $BF_3.OEt_2$ (76.5 μL) was added to the reaction mixture and allowed to stir under nitrogen atmosphere for 2 h. After 2 h, *p*-chloranil (4.5 mmol) was added, and the reaction mixture was stirred under reflux for 2 h. The solvent was removed under reduced pressure. The crude porphyrin was subjected to column chromatography (basic alumina). A purple-colored band eluted at 50:50 CH_2Cl_2/Hexane was identified as BTP. Yield: (~15%). Mp > 300°C. ^{1}H NMR (400 MHz, Chloroform-*d*): δ 9.12 (s, 8H), 8.14 (s, 4H), 8.14 – 8.04 (m, 8H), 7.67 – 7.54 (m, 8H), -2.59 (s, 2H). ^{13}C NMR (500 MHz, DMSO-d_6) δ 110.41, 112.56,

121.06, 124.08, 125.20, 131.10, 134.84, 155.03, 160.72, 186.39, 190.74, 165.61. IR (Neat): υ_{max} 3012, 2356, 2309, 1743, 1371, 1218 cm^{-1}. MALDI-TOF MS: *m*/*z* 839.2 $[M]^+$. Anal. Calcd for $C_{52}H_{30}N_4S_4$: C, 74.43; H, 3.60; N, 6.68; S, 15.29. Found: C, 74.02; H, 3.10; N, 6.38; S, 15.13.

2.4.3. Synthesis of 5, 10, 15, 20 – Tetrakis (3-sulfonatobenzo[b]thiophene) porphyrin (SBTP).

To synthesize SBTP, excess of chlorosulfonic acid (1.2 mL) was taken in a round-bottomed flask and 30 mg of BTP (0.04 mmol) in dry CH_2Cl_2 (10 mL) was added drop-wise under constant stirring at 0°C for 15 min. The reaction mixture was further stirred for 45 min at room temperature. The reaction mixture was monitored by TLC. After 1 h, excess acid was quenched and neutralized with diluted sodium hydroxide. The precipitate was collected and washed several times with methanol to extract a pure compound from other inorganic salts. The compound in methanol was concentrated under reduced pressure and collected as a brown powder. After the separation of salts, the crude mixture was purified by reverse phase column chromatography (C18 silica gel; MeOH: H_2O 50:50). To obtain the pure compound, the crude material from the previous column was purified by

semi-preparative reversed HPLC on a YMC-Triart, 5 μm, C18, 250 x 10 mm column with a gradient solvent system (from a 60 % aqueous methanol to 100 % methanol over 50 min, 0.1 % trimethylamine, flow rate: 2 mL/min, detection : UV 430 nm). The SBTP (30 mg, yield 5%) was eluted at 34 min under these conditions. Mp > 300°C. ^{1}H NMR (600 MHz, DMSO-d_6) δ 9.18 (s, 8H), 8.81 (s, 1H), 8.56 – 8.41 (m, 4H), 8.23 (d, J = 8.1 Hz, 4H), 7.94 (d, J = 7.5 Hz, 4H), 7.65 – 7.54 (m, 4H), -2.66 (s, 2H). ^{13}C NMR (600 MHz, DMSO-d_6) δ 112.6, 122.52, 123.06, 124.45, 132.48, 135.31, 138.99, 140.62, 142.06, 143.39, 165.61. IR (Neat): υ_{max} 3317, 3049, 2926, 1746, 1549, 1431, 1346, 1243, 1151, 1065 cm^{-1}. MALDI-TOF MS: *m*/*z* 1248 $[M+1]^{+}$. Anal. Calcd for $C_{52}H_{26}N_4Na_4O_{12}S_8$: C, 50.08; H, 2.10; N, 4.49. Found: C, 50.12; H, 2.13; N, 4.53. Chemical purity was assessed by HPLC: over 95.5 %.

2.4.4. MTT assay

MCF-7 cells were plated onto a 96-well plate and incubated at 37 ℃ in 5% CO_2 for 24 h. Cells were treated with SBTP at different concentrations () and incubated for 24 h. Later, cells were irradiated with 660 nm diode laser at 50 mW for 30 min. Cells were incubated at 37 ℃ in 5% CO_2 for 24 h. the cells were then treated with MTT solution (Thiazolyl Blue Tetrazolium

Bromide) and incubated at 37 ℃ in 5% CO_2 for 2 h. After removal of the MTT solution, DMSO (50 μL) was added for dissolving the formazan crystals. A multi-plate reader was used (Molecular Devices, Gemini XS) to measure the absorbance at 570 nm.

2.4.5. Intracellular uptake of SBTP by MCF-7 cells

MCF-7 cells were plated onto a 12-well plate and incubated at 37 ℃ in 5% $CO_2$for 24 h. SBTP was then added and cells were incubated at different time intervals and observed using a fluorescence microscope.

2.4.6. Intracellular localization assay

MCF-7 cells were seeded on cover-glass and incubated for 24 h at 37 ℃ in 5% CO_2. SBTP was then treated and cells were incubated at 37 ℃ in 5% CO_2 for 2 h. The medium was removed and cells were washed with 1x PBS. The cells were fixed in 4% formaldehyde for 15 min at room temperature. The cells were washed with 1X PBS, 0.2% saponin was added and incubated at room temperature for 10 min. Cells were then washed using 1X PBS, and stained with organelle-specific probes (Hoechst λexi: 350/λemi: 461, Alexa Fluor® 488 Phalloidin 488/525, Mito-Tracker 490/516)and

incubated at room temperature for 10 min in the dark. Cells were observed using Confocal Microscope (Nikon, Eclipse Ti-U/Yokogawa, CSU-X1).

2.4.7. Intracellular ROS generation

MCF-7 cells were plated onto a 12-well plate and incubated at 37 ℃ in 5% CO_2 for 24 h. Cells were then incubated with SBTP for 1 h and were irradiated with 660 nm diode laser at 30 mW for 10 min. MCF-7 cells were treated with 4% formaldehyde, and then incubated at room temperature for 10 min in the dark. Cells were washed with 1X PBSand treated with 2', 7'-dichlorofluorescin diacetate 20 μM, and incubated for 15 min at room temperature. Cells were observed using a fluorescence microscope with the excitation and emission wavelengths of 495 nm and 529 nm.

2.4.8. High-content screening assay

MCF-7 cells were treated with SBTP and irradiated at 50 mW for 30 min. Cells were treated with calcium indicator orange (Invitrogen, CA, USA), and incubated at room temperature in the dark for 45 min. Cells were then washed with 1X PBS and treated with Calceinacetoxymethyl ester (calcein-AM) in MitoProbe™ transition Pore Assay kit (Invitrogen, CA, USA).

Caspase-3 substrate was then added and cells were incubated at 37 ℃ in the dark for 6 min followed by the addition of $CoCl_2$ and incubation at 37 ℃ in the dark for 10 min. Cells were then washed with 1X PBS and excited at 488 nm. A built-in birefringent crystal of the acousto-optic tunable filter (AOTF, Brimrose Corporation, TEAF10-0.45-0.7-s, MD, USA) was detected by fluorescence. Images were analyzed using commercially available software (MetaMorph, Version 7.7, Molecular Devices, CA, USA).

2.4.9. Intrinsic/extrinsic apoptotic pathway studies

Caspase-3[(Z-DEVD)2-Magic Red], caspase-8[(Z-IETD)2-Rh110], and caspase-9[(Ac-LEHD)2-Rh110] substrates were purchased from Immunochemistry Technologies (MN, USA) and AnaSpec (CA, USA). Stock solutions were prepared according to the manufacturer's instructions. Cells were treated with a photosensitizer for concentration processing, and then cells were irradiated with a 660 nm diode laser at 50 mW for 30 min. Cells were then removed from the media and washed with 1X PBS. For caspase-8 inhibitor (z-IETD-fmk) and caspase-2 inhibitor (z-VDVAD-fmk) studies, cells were pre-incubated with inhibitors for 15 min, followed by SBTP treatment. Cells were incubated with 6 μM working solution of

caspase-8 or caspase-9 at 37 ℃ in the dark for 2 h. For the analysis of caspase-3, cells were washed, treated with 20 mM caspase-3, and incubated at 37 ℃ in the dark for 1 h. Cells were then washed with 1X PBS and observed using a fluorescence microscope using the excitation wavelength at 488 nm, and the emission wavelengths for caspase-3, caspase-8, and caspase-9 at 617, 523, and 523 nm, respectively.

2.5.0. DNA fragmentation assay

MCF-7 cells were treated with a photosensitizer and then irradiated at 50 mW for 30 min. Cells were washed with 1X PBS. To extract DNA from cells, QIAamp ® DNA Mini kit was used. DNA was extracted according to the manufacturer's instructions. 10 µL DNA was loaded with 6X loading buffer, and run on a 0.8% agarose gel electrophoresis in TBE buffer at 85 V for 1 h 30 min. LabChip® GXⅡ was used for detecting DNA fragments. Gel-Dye was prepared by adding DNA Dye to one vial of DNA Gel Matrix. Vortex and transfer mixture into two spin filters. Centrifuge at 9200 rcf for 7.5 min at room temperature. Rinsed and aspirated each Chip well twice with DW. Added DNA marker, DNA sample to Chip. Results were analyzed using LabChip® GXⅡ (PerkinElmer, USA).

References

1. Ferlay, J.; Soerjomataram, I.; Dikshit, R.; Eser, S.; Mathers, C.; Rebelo, M.; Parkin, D. M.; Forman, D.; Bray, F. Cancer incidence and mortality worldwide: Sources, methods and major patterns in GLOBOCAN 2012. *International Journal of Cancer* **2015,** 136, E359-E386.

2. Dolmans, D. E. J. G. J.; Fukumura, D.; Jain, R. K. Photodynamic therapy for cancer. *Nat. Rev. Cancer* **2003,** 3, 380-387.

3. Agostinis, P.; Berg, K.; Cengel, K. A.; Foster, T. H.; Girotti, A. W.; Gollnick, S. O.; Hahn, S. M.; Hamblin, M. R.; Juzeniene, A.; Kessel, D.; Korbelik, M.; Moan, J.; Mroz, P.; Nowis, D.; Piette, J.; Wilson, B. C.; Golab, J. Photodynamic therapy of cancer: An update. *Ca-Cancer J. Clin.* **2011,** 61, 250-281.

4. Brown, S. B.; Brown, E. A.; Walker, I. The present and future role of photodynamic therapy in cancer treatment. *Lancet Oncol.* **2004,** 5, 497-508.

5. Triesscheijn, M.; Baas, P.; Schellens, J. H.; Stewart, F. A. Photodynamic therapy in oncology. *Oncologist* **2006,** 11, 1034-44.

6. Huang, Z. A Review of Progress in Clinical Photodynamic Therapy. *Technology in cancer research & treatment* **2005,** 4, 283-293.

7. Bonnett, R. Photosensitizers of the porphyrin and phthalocyanine series for photodynamic therapy. *Chem. Soc. Rev.* **1995,** 24, 19-33.

8. Karunakaran, S. C.; Babu, P. S. S.; Madhuri, B.; Marydasan, B.; Paul, A. K.; Nair, A. S.; Rao, K. S.; Srinivasan, A.; Chandrashekar, T. K.; Rao, C. M.; Pillai, R.; Ramaiah, D. In Vitro Demonstration of Apoptosis Mediated Photodynamic Activity and NIR Nucleus Imaging through a Novel Porphyrin. *ACS Chem. Biol.***2013,** 8, 127-132.

9. Lang, K.; Mosinger, J.; Wagnerová, D. M. Photophysical properties of porphyrinoid sensitizers non-covalently bound to host molecules; models for photodynamic therapy. *Coord. Chem. Rev.* **2004,** 248, 321-350.

10. Jin, C. S.; Cui, L.; Wang, F.; Chen, J.; Zheng, G. Targeting-Triggered Porphysome Nanostructure Disruption for Activatable Photodynamic Therapy. *Adv. Healthcare Mater.* **2014,** 3, 1240-1249.

11. Lipson, R. L.; Baldes, E. J.; Olsen, A. M. Hematoporphyrin derivative: a new aid for endoscopic detection of malignant disease. *J. Thorac. Cardiovasc.Surg.* **1961,** 42, 623-9.

12. Wilson, B. C.; Olivo, M.; Singh, G. Subcellular Localization of Photofrin and Aminolevulinic Acid and Photodynamic Cross-Resistance in Vitro in Radiation-Induced Fibrosarcoma Cells Sensitive or Resistant to

Photofrin-Mediated Photodynamic Therapy. *Photochem. Photobiol.* **1997,** 65, 166-176.

13. Josefsen, L. B.; Boyle, R. W. Photodynamic therapy: novel third-generation photosensitizers one step closer? *Br. J. Pharmacol.* **2008,** 154, 1-3.

14. Moan, J.; Berg, K. The photodegradation of porphyrins in cells can be used to estimate the lifetime of singlet oxygen. *Photochem. Photobiol.* **1991,** 53, 549-553.

15. Dougherty, T. J.; Gomer, C. J.; Henderson, B. W.; Jori, G.; Kessel, D.; Korbelik, M.; Moan, J.; Peng, Q. Photodynamic therapy. *J. Natl. Cancer Inst.* **1998,** 90, 889-905.

16. Elmore, S. Apoptosis: a review of programmed cell death. *Toxicol. Pathol.* **2007,** 35, 495-516.

17. Wang, X. The expanding role of mitochondria in apoptosis. *Genes Dev.* **2001,** 15, 2922-33.

18. Gogvadze, V.; Orrenius, S.; Zhivotovsky, B. Mitochondria in cancer cells: what is so special about them? *Trends Cell Biol.* **2008,** 18, 165-73.

19. Modica-Napolitano, J. S.; Singh, K. K. Mitochondrial dysfunction in cancer. *Mitochondrion* **2004,** 4, 755-62.

20. Wallace, D. C. Mitochondria and cancer. *Nat. Rev. Cancer* **2012,** 12, 685-698.

21. Kroemer, G.; Pouyssegur, J. Tumor cell metabolism: cancer's Achilles' heel. *Cancer Cell* **2008,** 13, 472-82.

22. Bellance, N.; Lestienne, P.; Rossignol, R. Mitochondria: from bioenergetics to the metabolic regulation of carcinogenesis. *Front. Biosci., Landmark Ed.* **2009,** 14, 4015-34.

23. Young, D. W.; Bender, A.; Hoyt, J.; McWhinnie, E.; Chirn, G. W.; Tao, C. Y.; Tallarico, J. A.; Labow, M.; Jenkins, J. L.; Mitchison, T. J.; Feng, Y. Integrating high-content screening and ligand-target prediction to identify mechanism of action. *Nat. Chem. Biol.* **2008,** 4, 59-68.

24. Schembri, L.; Zanese, M.; Depierre-Plinet, G.; Petit, M.; Elkaoukabi-Chaibi, A.; Tauzin, L.; Florean, C.; Lartigue, L.; Medina, C.; Rey, C.; Belloc, F.; Reiffers, J.; Ichas, F.; De Giorgi, F. Recombinant differential anchorage probes that tower over the spatial dimension of intracellular signals for high content screening and analysis. *Anal. Chem.* **2009,** 81, 9590-8.

25. Lindsey, J. S.; Schreiman, I. C.; Hsu, H. C.; Kearney, P. C.; Marguerettaz, A. M. Rothemund and Adler-Longo reactions revisited:

synthesis of tetraphenylporphyrins under equilibrium conditions. *J. Org. Chem.* **1987,** 52, 827-836.

26. Monteiro, C. J. P.; Pereira, M. M.; Pinto, S. M. A.; Simões, A. V. C.; Sá, G. F. F.; Arnaut, L. G.; Formosinho, S. J.; Simões, S.; Wyatt, M. F. Synthesis of amphiphilic sulfonamide halogenated porphyrins: MALDI-TOFMS characterization and evaluation of 1-octanol/water partition coefficients. *Tetrahedron* **2008,** 64, 5132-5138.

27. Fleischer, E. B.; Palmer, J. M.; Srivastava, T. S.; Chatterjee, A. Thermodynamic and kinetic properties of an iron-porphyrin system. *J. Am. Chem. Soc.* **1971,** 93, 3162-7.

28. Seybold, P. G.; Gouterman, M. Porphyrins: XIII: Fluorescence spectra and quantum yields. *Journal of Molecular Spectroscopy* **1969,** 31, 1-13.

29. Thomas, A. P.; Saneesh Babu, P. S.; Asha Nair, S.; Ramakrishnan, S.; Ramaiah, D.; Chandrashekar, T. K.; Srinivasan, A.; Radhakrishna Pillai, M. meso-Tetrakis(p-sulfonatophenyl)N-Confused Porphyrin Tetrasodium Salt: A Potential Sensitizer for Photodynamic Therapy. *Journal of Medicinal Chemistry* **2012,** 55, 5110-5120.

30. Malik, Z.; Amit, I.; Rothmann, C. Subcellular localization of sulfonated tetraphenyl porphines in colon carcinoma cells by spectrally resolved imaging. *Photochem Photobiol* **1997,** 65, 389-96.

31. Rapozzi, V.; Zorzet, S.; Zacchigna, M.; Della Pietra, E.; Cogoi, S.; Xodo, L. Anticancer activity of cationic porphyrins in melanoma tumour-bearing mice and mechanistic in vitro studies. *Molecular Cancer* **2014,** 13, 75.

32. Paul, A.; Eun, C.-J.; Song, J. M. Cytotoxicity mechanism of non-viral carriers polyethylenimine and poly-l-lysine using real time high-content cellular assay. *Polymer* **2014,** 55, 5178-5188.

33. Morishima, S.; Shibata, M. A.; Ohmichi, M.; Otsuki, Y. Raloxifene, a selective estrogen receptor modulator, induces mitochondria-mediated apoptosis in human endometrial carcinoma cells. *Med. Mol. Morphol.* **2008,** 41, 132-8.

34. Alonso, M. M.; Asumendi, A.; Villar, J.; Gil, M. J.; Martinez-Merino, V.; Encio, I. J.; Migliaccio, M. New benzo(b)thiophenesulphonamide 1,1-dioxide derivatives induce a reactive oxygen species-mediated process of apoptosis in tumour cells. *Oncogene* **2003,** 22, 3759-69.

35. Sulfonation and chlorosulfonation of aromatic compounds using chlorosulfonic acid. In *Chlorosulfonic Acid: A Versatile Reagent*, Cremlyn, R. J., Ed. The Royal Society of Chemistry: 2002; pp 35-145.

36. Bassin, J. P.; Cremlyn, R. J.; Swinbourne, F. J. Chlorosulfonation of aromatic and hetero-aromatic systems. *Phosphorus, Sulfur Silicon Relat. Elem.***1991,** 56, 245-275.

37. Saltsman, I.; Mahammed, A.; Goldberg, I.; Tkachenko, E.; Botoshansky, M.; Gross, Z. Selective Substitution of Corroles: Nitration, Hydroformylation, and Chlorosulfonation. *J. Am. Chem. Soc.* **2002,** 124, 7411-7420.

38. Ethirajan, M.; Chen, Y.; Joshi, P.; Pandey, R. K. The role of porphyrin chemistry in tumor imaging and photodynamic therapy. *Chem. Soc. Rev.* **2011,** 40, 340-362.

39. Prasanth, C. S.; Karunakaran, S. C.; Paul, A. K.; Kussovski, V.; Mantareva, V.; Ramaiah, D.; Selvaraj, L.; Angelov, I.; Avramov, L.; Nandakumar, K.; Subhash, N. Antimicrobial Photodynamic Efficiency of Novel Cationic Porphyrins towards Periodontal Gram-positive and Gram-negative Pathogenic Bacteria. *Photochem. Photobiol.***2014,** 90, 628-640.

40. Castano, A. P.; Demidova, T. N.; Hamblin, M. R. Mechanisms in photodynamic therapy: part one-photosensitizers, photochemistry and cellular localization. *Photodiagn. Photodyn. Ther.* **2004,** 1, 279-93.

41. Oleinick, N. L.; Morris, R. L.; Belichenko, I. The role of apoptosis in response to photodynamic therapy: what, where, why, and how. *Photochem. Photobiol. Sci.* **2002,** 1, 1-21.

42. Patito, I. A.; Rothmann, C.; Malik, Z. Nuclear transport of photosensitizers during photosensitization and oxidative stress. *Biol. Cell* **2001,** 93, 285-91.

43. Roding, J.; Naujok, A.; Zimmermann, H. W. Effects of ethidium bromide, tetramethylethidium bromide and betaine B on the ultrastructure of HeLa cell mitochondria in situ. A comparative binding study. *Histochemistry* **1986,** 85, 215-22.

44. Woodburn, K. W.; Vardaxis, N. J.; Hill, J. S.; Kaye, A. H.; Phillips, D. R. Subcellular localization of porphyrins using confocal laser scanning microscopy. *Photochem Photobiol* **1991,** 54, 725-32.

45. Woodburn, K. W.; Vardaxis, N. J.; Hill, J. S.; Kaye, A. H.; Reiss, J. A.; Phillips, D. R. Evaluation of porphyrin characteristics required for photodynamic therapy. *Photochem Photobiol* **1992,** 55, 697-704.

46. Li, Y.; Geyer, C. R.; Sen, D. Recognition of anionic porphyrins by DNA aptamers. *Biochemistry* **1996,** 35, 6911-22.

47. Ning, J.; Wang, Y.; Wu, Q.; Zhang, X.; Lin, X.; Zhao, H. Novel supramolecular assemblies of repulsive DNA-anionic porphyrin complexes based on covalently modified multi-walled carbon nanotubes and cyclodextrins. *RSC Advances* **2015,** 5, 21153-21160.

48. Lauceri, R.; Purrello, R.; Shetty, S. J.; Vicente, M. G. Interactions of anionic carboranylated porphyrins with DNA. *J Am Chem Soc* **2001,** 123, 5835-6.

49. Moor, A. C. Signaling pathways in cell death and survival after photodynamic therapy. *J. Photochem. Photobiol., B* **2000,** 57, 1-13.

50. Kim, J.-A.; Han, E.; Eun, C.-J.; Tak, Y. K.; Song, J. M. Real-time concurrent monitoring of apoptosis, cytosolic calcium, and mitochondria permeability transition for hypermulticolor high-content screening of drug-induced mitochondrial dysfunction-mediated hepatotoxicity. *Toxicol. Lett.* **2012,** 214, 175-181.

51. Kaina, B. DNA damage-triggered apoptosis: critical role of DNA repair, double-strand breaks, cell proliferation and signaling. *Biochem. Pharmacol.* **2003,** 66, 1547-54.

52. Roos, W. P.; Kaina, B. DNA damage-induced cell death by apoptosis. *Trends Mol. Med.* **2006,** 12, 440-50.

53. Houghton, J. A.; Harwood, F. G.; Tillman, D. M. Thymineless death in colon carcinoma cells is mediated via fas signaling. *Proc. Natl. Acad. Sci. U. S. A.* **1997,** 94, 8144-9.

54. Nagane, M.; Pan, G.; Weddle, J. J.; Dixit, V. M.; Cavenee, W. K.; Huang, H. J. Increased death receptor 5 expression by chemotherapeutic agents in human gliomas causes synergistic cytotoxicity with tumor necrosis factor-related apoptosis-inducing ligand in vitro and in vivo. *Cancer Res.***2000,** 60, 847-53.

55. Wen, J.; Ramadevi, N.; Nguyen, D.; Perkins, C.; Worthington, E.; Bhalla, K. Antileukemic drugs increase death receptor 5 levels and enhance Apo-2L-induced apoptosis of human acute leukemia cells. *Blood* **2000,** 96, 3900-6.

56. Beurel, E.; Kornprobst, M.; Blivet-Van Eggelpoel, M. J.; Ruiz-Ruiz, C.; Cadoret, A.; Capeau, J.; Desbois-Mouthon, C. GSK-3beta inhibition by lithium confers resistance to chemotherapy-induced apoptosis through the repression of CD95 (Fas/APO-1) expression. *Exp. Cell Res.* **2004,** 300, 354-64.